MODIFIED DIRECT TORQUE CONTROL OF INDUCTION MOTOR DRIVES

By

AMALI DEHIGOLLE GEDARA

Bachelor of Science in Electrical & Electronics Engineering

University of Peradeniya

Sri Lanka

2014

Submitted to the Faculty of the
Graduate College of the
Oklahoma State University
in partial fulfillment of
the requirements for
the Degree of
MASTER OF SCIENCE
July, 2018

MODIFIED DIRECT TORQUE CONTROL OF

INDUCTION MOTOR DRIVES

Thesis Approved:

Dr. Nishantha C. Ekneligoda

Thesis Adviser

Dr. R. Ramakumar

Dr. John O'Hara

ACKNOWLEDGEMENT

I would like to express my sincere gratitude to Dr. Nishantha Ekneligoda for his constant support, guidance, and encouragement throughout this study. Then, I would like to thank Dr. R. Ramakumar and Dr. John O'Hara for serving on my committee. The comments and the guidance offered by the committee members are sincerely appreciated.

Next, I would like to thank Dr. Jeffery Young, the department chair, Electrical and Computer Engineering and the staff members for their support provided during my study period. Further, this project would not be completed without receiving the financial support from Airplane Transporting Systems (ATS) and High Energy Physics group. I would like to express my gratitude to them for providing financial assistance throughout my study period.

I also wish to thank my parents and my family for their never-ending support and encouragement.

Amali Dehigolle Gedara.

7/18/18

Name: AMALI DEHIGOLLE GEDARA

Date of Degree: JULY, 2018

Title of Study: MODIFIED DIRECT TORQUE CONTROL OF INDUCTION MOTOR DRIVES

Major Field: Electrical Engineering

Abstract: Over past years, direct torque control (DTC) has proven to be a powerful technique for controlling induction motors since, its simple structure, fast performance, and robustness. However, conventional DTC has a major problem in selecting the optimum voltage vector in order to provide fast torque response, due to the nature of the hysteresis controller. This thesis presents a new control topology for DTC, which enables fast torque response and reduced steady state ripple. The proposed scheme utilizes an optimized inverter voltage vector selection process ensuring a higher rate of torque increment during transient periods. Further, two nonlinear adaptation mechanisms are used to replace the hysteresis controllers thus obtain enhanced torque and stator flux regulation. One scheme is based on sliding mode theory and the other method is based on fuzzy logic strategy. A comprehensive simulation study has been performed to evaluate the performances of the proposed sector-advancing algorithm under the two nonlinear control methodologies. The corresponding simulation results and discussion are presented for each section. It is concluded that the proposed DTC algorithms with sliding mode and fuzzy logic strategies demonstrate better characteristics in both transient and steady state operation with regards to the conventional DTC.

TABLE OF CONTENTS

Chapter Page

LIST OF TABLES

Table Page

LIST OF FIGURES

Figure Page

ABBREVIATIONS

AC	Alternative current
AI	Artificial intelligent
CDTC	Conventional direct torque control
BJT	Bipolar junction transistor
DC	Direct current
DTC	Direct torque control
FIS	Fuzzy inference system
FL	Fuzzy logic
FLC	Fuzzy logic control
FLDTC	Fuzzy logic direct torque control
FOC	Field-oriented control
GTO	Gate turn-off thyristors
IGBT	Insulated-gate bipolar transistor
IGCT	Integrated gate-commutated thyristor
IM	Induction motor
MF	Membership function
MOS	Metal Oxide Semiconductor
MOSFET	Metal-oxide-semiconductor field-effect transistor
PC	Predictive control
PI	Proportional-integral
PWM	Pulse width modulation
SA	Sector advancing
SM	Sliding mode
SMC	Sliding mode control
SMDTC	Sliding mode direct torque control
v/f	Voltage-by-frequency

VSI	Voltage source inverter
VSC	Variable structure control

CHAPTER I

INTRODUCTION

1.1 Background

Induction motors are the most commonly used electric machines in the industry, which is an ingenious discovery of the late nineteenth century. Being a robust and rugged machine, three phase induction motor still maintains its incomparable popularity in process of electrical to mechanical power conversion. Induction motors were primarily used in constant speed motor drives. Earlier, dc motors were the only motor used for the applications which require a wide range of speed. However, the rapid development of the power electronic devices and control techniques has given rise to the high performance variable speed induction motor drives. Vector control technique which is also known as field oriented control (FOC) has made a major difference in terms of dynamic performance of induction machine [1, 2]. Vector control permits induction motor to control similar to the separately excited dc motor. Recent advances in artificial intelligent (AI) techniques, including fuzzy logic (FL), neural network, genetic algorithm, and expert systems have contributed to the performance improvement of the induction motor drives [3-5]. Speed sensorless operation of induction motor drives has also gained the research attention over the past years.

1.1.1 Evolution of Motor Control and Power Electronic Devices

The development of motor control from dc drives to various forms of ac drives has been motivated by the need for the high performance drives with improved quality and reliable operation in numerous applications. Evolution of one form to another strive to enhance the existing advantages while getting rid of the disadvantages. Fig. 1.1 shows the simplistic viewpoint of drive evolution as four steps [6]. Where V and f denote the

voltage and frequency. Comparison of control techniques and the controller performance are presented in Table 1.1.

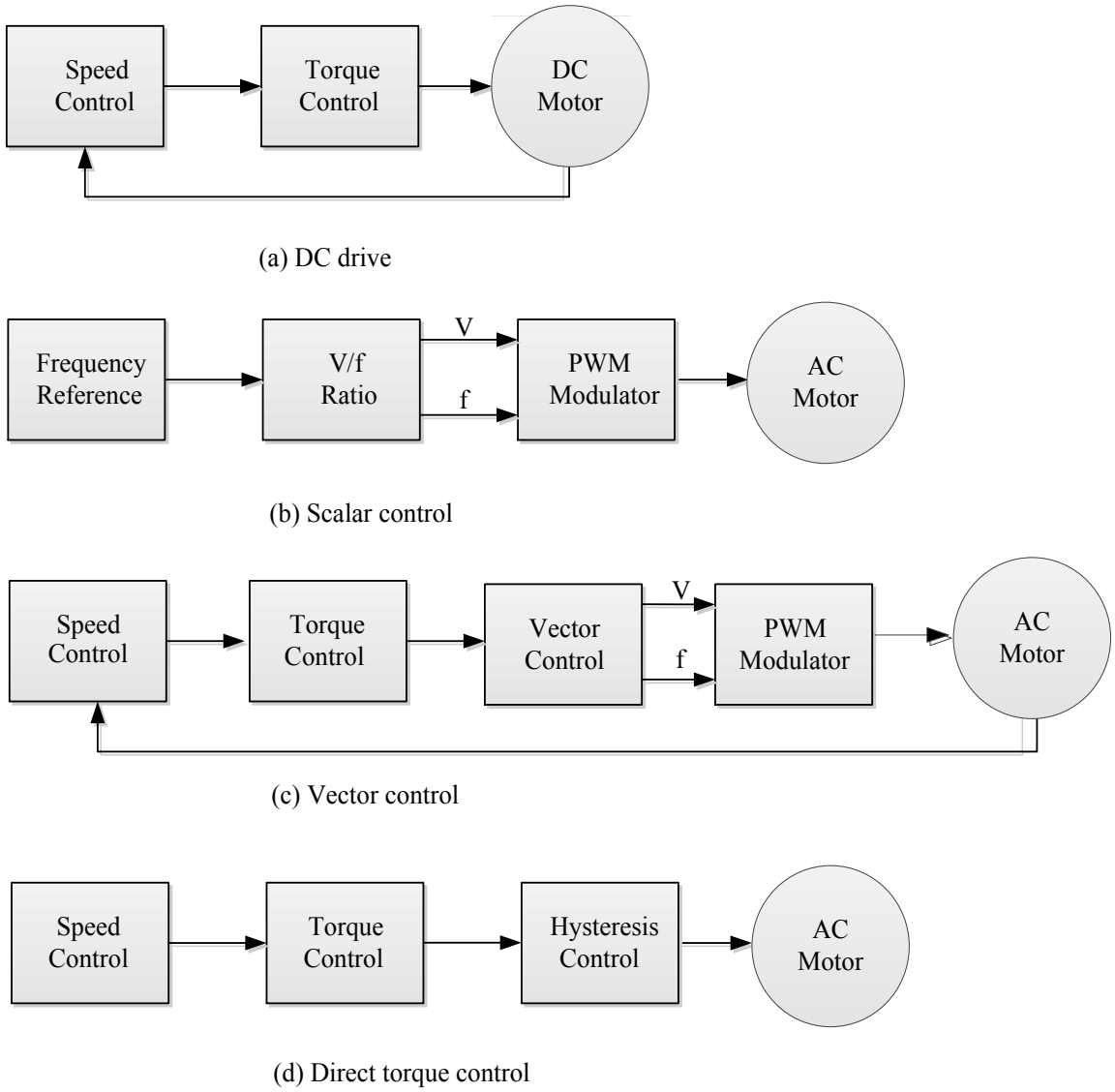

Fig. 1.1. Evolution of electric drive control techniques.

Moreover, power electronics and semiconductor devices have gone through a dynamic evolution in the recent years due to many innovations in that field. The evolution of power electronics can be identified as four generations: thyristor era, self-controlled power devices (BJT, power MOSFETs, and GTOs), the introduction of IGBT, and the current generation of IGCTs and MOSs [7]. These trends of power semiconductor

devices have been paved the way for designing high-performance motor drives. Power MOSFETs and IGBTs are extremely important in the field of motor drives. In particular, IGBTs are used for multi-level inverters since they are capable of handling high voltage [8, 9].

TABLE 1.1

Comparison of the Existing Motor Control Methods [6]

Control method	Flux Control	Torque control	Advantages	Disadvantages
DC drives	Direct	Direct	Simple. Better torque response. High precision.	High maintenance. High motor cost. For higher precision an encoder is required.
Scalar Control	None	None	Simple. No encoder is required.	Low precision. Poor torque response.
Vector control	Indirect	Direct	Better torque response. High precision.	Encoder is always required.
Direct torque control	Direct	Direct	Excellent torque response. No encoder is required. Moderate precision.	For higher precision an encoder is required.

1.1.1 Scalar Control

The scalar controllers are inherently simple, low cost, and low performance drives, which do not require complex signal processing as in vector control methods [10]. In scalar control, the speed of the induction motor is controlled by adjusting the magnitude or the frequency of the stator voltage or current. The studies of scalar control consist of open loop v/f control, closed loop v/f control, stator current and slip frequency control [11]. The variable frequency motor drives with open loop v/f control are an ideal match for the constant torque applications where there is no restriction upon the speed regulation[3]. When the drive requires precision speed or torque control with faster dynamic performance, it is essential to function the motor in closed loop mode.

1.1.2 Vector Control

Vector controllers are relatively expensive high performance drives, in which the control action is obtained by controlling the magnitude, frequency, and phase of stator current. Vector control includes two control methods namely, field oriented control (FOC) and direct self control (DSC). The fundamental idea behind the FOC is to control the stator currents by representing them as vectors in rotating reference frame [9]. Even though vector control technique has many advantages, it suffers from unavoidable drawbacks such as, low precision due to the high computation complexity, difficulty of the indirect control in contrast to direct control, and multiple extra current regulators [10].

1.1.3 Direct Torque Control

In order to improve the accuracy and to relax the complexity of the traditional FOC, various novel alternative techniques have been proposed. Among them, one of the breakthroughs was the introduction of direct torque control (DTC) [11]. Similar to the FOC techniques, DTC was also initially established from the field geometry principle [11].

Due to its simplicity, fast dynamics, and robustness against machine parameters and perturbations, DTC is attractive in contrast to the FOC and most of the other traditional control methods [12]. However, there are a few drawbacks in the conventional DTC (CDTC) methodology. Some of the major issues are its undesirable torque ripple which causes noise and increased losses to the drive [13] and difficulties in selecting optimum voltage vector to give desired characteristics. Nevertheless, a number of attempts have been made to overcome these drawbacks by introducing improved DTC algorithms.

1.2 Review of Previous Work

Research interest in induction motor (IM) control has grown significantly over the past few decades [12, 14-19]. Researchers have devoted a lot of effort to develop new control strategies, algorithms, and hardware for IM control. After introducing the DTC concept in 1986 by Takahashi and Noguchi [20], researchers have devoted a great effort to improve the performance of the CDTC scheme by integrating advanced control

techniques. Some of the recent advancements of the DTC are presented in [15-25]. Improvements in IM controls are briefly discussed in the following section under four sub categories namely, nonlinear control, intelligent control, speed sensorless control and predictive control.

1.2.1 Nonlinear Control

Nonlinear control algorithms are well suited for IM control since they capture high amount of system dynamics of the plant. Most popular nonlinear control methods applied in IM control are variable structure control (VSC), feedback linearization and backstepping control [16, 26, 27]. The VSC or so called sliding mode control (SMC) is known for its robustness and disturbance rejection in nonlinear control arena [14]. Therefore, integration of VSC with the DTC can be found in the literature [12, 14-16, 28-30]. Online adaptive VSC method for IM direct speed and flux control based on the FOC has been proposed in [15]. Here, the adaptive rotor flux and speed controller works under VSC principle with unknown, time varying load torque and rotor resistance. Employing a sliding mode observer based on a dual reference frame motor model, a complete VSC direct torque and flux control methodology has been introduced in [12] for sensorless IM drives. With this improved VSC-DTC mechanism, steady state torque, flux and current pulsation are significantly reduced compared to the CDTC. A voltage source inverter (VSI) based DTC have been addressed in [30] with SMC strategy to improve the performance of CDTC. The corresponding voltage vector has been generated by two methods which are the direct or the high performance hysteresis VSI and indirect or the space vector modulation VSI.

Combination of feedback linearization with SMC for IM DTC has been proposed in [16]. Here, feedback linearization has been introduced to make a decoupled linear IM model with torque and speed magnitude. Based upon this model, SMC has been employed to obtain ripple free, robust and fast torque and flux control actions. Application of input-output feedback linearization in space vector modulated adjustable speed sensorless DTC drive can be found in [17]. Here, the feedback linearization control has been utilized to properly select the inverter reference voltage, considering stator current and flux vectors as state variables in the rotating reference frame.

Integration of the integrator backstepping DTC has been proposed in [18] for efficiency optimization of IMs. Here, the model based loss minimization method combined with a backstepping controller has been introduced in the stationary reference frame with the aid of a SMC observer. A nonlinear backstepping controller has been introduced to direct torque and flux control of a six-phase asymmetrical speed and voltage sensorless IM drive in [19]. Here, Lyapunov based decoupled torque and flux controllers are obtained in stationary reference frame and the space vector PWM technique has been employed to control the drive.

1.2.2 Intelligent Control

In recent years, more attention has been posed to machine learning, artificial intelligence (AI) and autonomous control of dynamical systems [31, 32]. Hence, the integration of control methodologies based on AI with DTC to enhance the performance and to improve the robustness becomes popular [4, 28, 33-35]. Among the wide range of intelligent algorithms, fuzzy-logic control (FLC) is one of the simplest methodology which does not require extensive mathematical analysis [33].

In order to obtain better transient and steady state performance of DTC drives, a proportional-integral (PI) controller and FL controller based method has been proposed in [4]. In this method, switching between the PI controller and the FLC is determined by the measured speed error of the machine. However, the switching limit depends on the type of the FLC which is being used, and hence the switching transition becomes more complex. The FLC based DTC algorithm proposed in [28] selects the bandwidth of the torque hysteresis controller such that it optimizes the torque ripple level. In order to reduce undesirable torque ripple in CDTC, authors in [34] have been proposed an FLC based approach to obtain optimum duty ratios of switching states using an analytical online algorithm.

1.2.3 Speed Sensorless Control

Speed sensorless control of IMs is a novel and promising research trend. Typically, all the IM states are not available for measurement, and hence an observer is employed to estimate the unknown states of the system [19, 21, 22]. In position/speed sensorless

control, speed or the position of the motor is estimated based on the machine parameters and the terminal voltage and current measurements [3, 11]. To realize high performance speed sensorless control of IM drives, various novel techniques have been proposed in literature [21, 36]. In order to avoid the variable switching problem in DTC, a constant switching frequency based speed sensorless control method has been proposed in [21]. In this approach, speed sensorless induction motor drive based on the DTC scheme is developed to maintain a constant switching frequency while the stator flux components are treated as control variables. Based on the space vector modulation technique a reformed DTC scheme for IM speed sensorless drive is introduced in [36]. Sliding mode observer (SMO) is a good solution for the speed sensorless IM control due to its fast dynamic response and resistance to the disturbances [26, 27, 37]. A number of different SMOs for IM speed sensorless control can be found in [22, 26, 27, 37-39]. Among them, speed observers are the most prominent. For instance, combined DTC algorithm with the SMO for improved IM operations is proposed in [12] which does not require speed information.

1.2.4 Predictive Control

Recently, Predictive control (PC) has been given great attention in research communities, and it has been shown that PC is one of the most promising robust control techniques for both linear and nonlinear systems. The notion of integrating PC with the advance IM control strategies such as DTC has been proposed [23, 24, 40-42]. In [23], a PC scheme which can be used for flux and torque control of H- bridge multilevel inverter fed IM is presented. The proposed method employs a proportional-integral (PI) type controller to achieve better steady state performance and a one-step predictive controller to obtain fast torque response.

A novel predictive DTC scheme for IM drives is proposed in [40]. The control scheme comprised of a Kalman filter based flux estimator and a predictive speed controller combined with a load torque observer for speed tracking. The control algorithm improves the performance of the IM drive in terms of speed trajectory tracking, flux and torque dynamic response and disturbance rejection. In [41], a predictive torque control algorithm

has been established based on instantaneous flux control. The new predictive torque control methodology exhibits lower switching frequency and better dynamic torque response with compared to traditional drive control techniques. Authors in [42] have developed a predictive torque control scheme using discrete time state space model of the IM including the time varying nature of the rotor speed. In this proposed control algorithm, the machine model is updated at each sampling state by evaluating a cost function. Based on the simplified finite state predictive torque control method, a modified DTC controller has been developed in [24]. This newly proposed method relaxes both the computational burden and the number of voltage vectors to be predicted compared to the traditional finite state predictive torque control.

1.3 Thesis Overview

In this thesis, a modified control algorithm is developed based on the sector advancing (SA) concept combining sliding-mode (SM) and fuzzy-logic (FL) nonlinear control methods. The conventional SA algorithm is available in the literature with traditional DTC drives [43, 44]. With regard to the traditional inverter vector selection process, the SA strategy allow fast transient response in torque control. The combined SA and nonlinear adaptation mechanisms are proposed to improve the dynamic performance of the DTC drive. The performance of the conventional and proposed DTC schemes are compared with a detail simulation study.

The rest of the thesis is organized as follows. Chapter II presents dynamic modeling of the induction motor including classical motor principle, reference frame theory, and two axes IM model in the stationary reference frame. The fundamental principle behind the DTC technique is illustrated in Chapter III. Further, a nonlinear control method; SMC and an intelligent control method; FLC techniques are discussed briefly. These two control mechanisms are used to improve the conventional DTC algorithm which is described in future chapters. Chapter IV gives the mathematical formulation of the proposed approach including sector advancing (SA) concept and the design procedure of FL and SM based torque and flux regulation for modified DTC method. Performance validation of the proposed scheme with respect to the CDTC algorithm and series of simulation test cases are provided in chapter V. These computer simulations are carried

out in MATLAB/ Simulink environment. Finally, the Chapter VI concludes the thesis with a summary of work carried out and the possible future directions.

CHAPTER II

MODELING OF INDUCTION MACHINE

2.1 Introduction

Unlike DC or synchronous motors, the physical arrangement of an induction motor is simple, as they do not require commutators, brushes, permanent magnet, etc. The name, induction is for the reason that the rotor voltage is induced in rotor winding without any external excitation method. The rotor of the induction motor can be identified as two ways, namely squirrel-cage rotors, which constitute a majority of induction motors and wound rotor type rotors which are the less common type of induction machines which are used only in the particular applications. The squirrel cage rotors are composed of conducting bars, which are shorted at the end using a ring while in wound rotors, the rotor windings are taken out and shorted at the slip rings using external resistors. The behavior of such induction motors can be reasonably approximated by an equivalent circuit which is discussed in this chapter.

2.2 Dynamic Modeling of Symmetrical Three-Phase Induction Motor

Three phase squirrel cage induction motors have been widely used in the industry since they are reliable, rugged in design, and economical. One of the major requirements of industry is to run the motor at different speeds and loads, which makes induction motor to be the first choice. The goal in this section is to establish a mathematical model that permits understanding the function of motor and employ that model in controller design of future chapters.

2.2.1 Reference Frame Theory

In some design and analysis of electrical machines, it is more convenient to use different reference frame to reduce the complexity of the modeling. Transforming the parameters to another reference frame eliminates the rotor position dependency of inductances and allows ac quantities to be treated as dc quantities. This idea establishes the framework of most controller design. In this transformation, all the machine variables are referred to a reference frame, which rotates at an arbitrary angular frequency.

Reference frame theory had been evolving since the late 1930s. Park, Stanley, Kron and Brereton el at. introduced changes of variable to eliminate the time-varying inductances in the voltage equations of induction machine which were suitable for a particular application. Each of these transformations was considered separately until developing one general transformation in 1965 which lumped all known transformations. In this, general transformation, stator and rotor variables are referred to a reference frame so-called arbitrary reference frame, which rotates at any arbitrary angular frequency or remains stationary. Every other transformation can be derived by setting the appropriate angular frequency. In this analysis, transformation of the three-phase symmetrical induction motor to the arbitrary reference frame is presented and then by assigning appropriate angular frequency the stationary reference frame model is derived [45]. Fig. 2.1 shows the winding arrangement and corresponding parameters of the stator and rotor circuit.

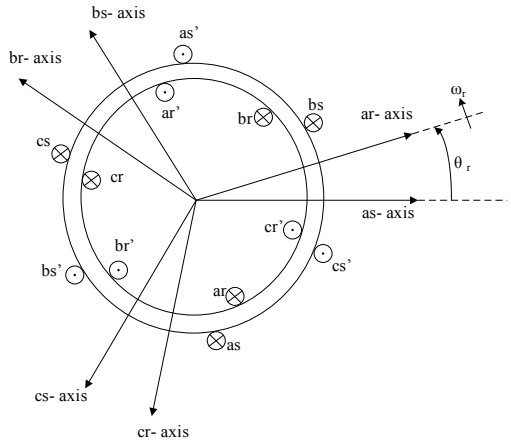

(a)

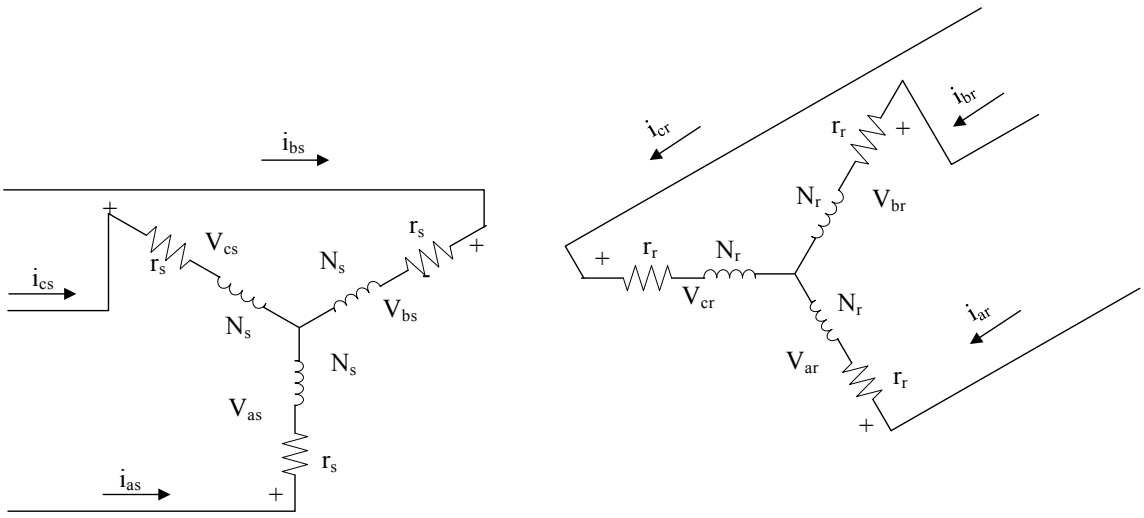

(b)

Fig. 2.1 Stator and rotor winding arrangement (a) Cross sectional view (b) Stator and rotor circuits.

Transformation of stationary three phase variables to the arbitrary reference frame can be expressed as [45],

$$f_{qd0s} = K_s f_{abcs} \tag{2.1}$$

$$\left(f_{qd0s}\right)^T = \left[f_{qs}\ f_{ds}\ f_{0s}\right] \tag{2.2}$$

$$(f_{abcs})^T = [f_{as}\ f_{bs}\ f_{cs}] \tag{2.3}$$

$$K_s = \frac{2}{3}\begin{bmatrix} \cos\theta & \cos\left(\theta - \frac{2\pi}{3}\right) & \cos\left(\theta + \frac{2\pi}{3}\right) \\ \sin\theta & \sin\left(\theta - \frac{2\pi}{3}\right) & \sin\left(\theta + \frac{2\pi}{3}\right) \\ \frac{1}{2} & \frac{1}{2} & \frac{1}{2} \end{bmatrix} \tag{2.4}$$

Transformation of rotor circuit to the arbitrary reference frame can be expressed as

$$f_{qd0r} = K_r f_{abcr} \tag{2.5}$$

$$\left(f_{qd0r}\right)^T = \left[f_{qr}\ f_{dr}\ f_{0r}\right] \tag{2.6}$$

$$(f_{abcr})^T = [f_{ar}\ f_{br}\ f_{cr}] \tag{2.7}$$

$$K_r = \frac{2}{3}\begin{bmatrix} \cos\beta & \cos\left(\beta - \frac{2\pi}{3}\right) & \cos\left(\beta + \frac{2\pi}{3}\right) \\ \sin\beta & \sin\left(\beta - \frac{2\pi}{3}\right) & \sin\left(\beta + \frac{2\pi}{3}\right) \\ \frac{1}{2} & \frac{1}{2} & \frac{1}{2} \end{bmatrix} \tag{2.8}$$

where,

$$\beta = \theta - \theta_r \tag{2.9}$$

$$\theta = \int \omega\, dt \tag{2.10}$$

where, θ is the angular displacement and ω is the angular velocity of the arbitrary reference frame. θ_r is the angular displacement of the rotor with respect to the stator. In above equations, f is used to represent any of these quantities such as voltage, current and flux linkage of the induction machine. The superscript T denotes the transpose of the vector while subscripts a, b, and c use to represent the three phase quantities and q, d, and 0 denote the coordinates of arbitrary reference frame. The subscript s denotes variables corresponding to the stator circuit and subscript r represents the variables of the rotor circuit. K_s and K_r are the stator and rotor transformation matrices respectively.

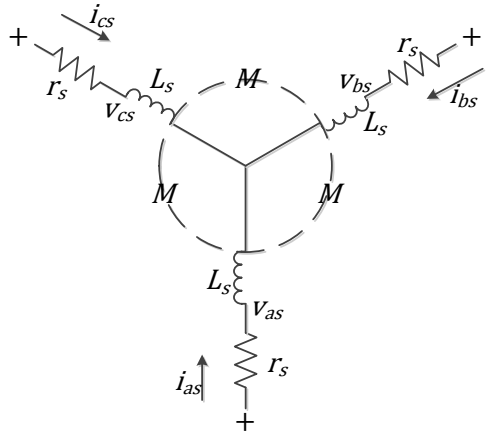

Fig. 2.2 Stator winding arrangement of a symmetrical induction machine.

According to the Fig. 2.2, the voltage in each phase of the stationary stator circuit can be written as the sum of the voltages across stator inductor L_s and the stator resistor r_s.

$$v_{as} = v_{aRs} + v_{aLs} \tag{2.11}$$

$$v_{bs} = v_{bRs} + v_{bLs} \tag{2.12}$$

$$v_{cs} = v_{cRs} + v_{cLs} \tag{2.13}$$

Stator phase voltages in the arbitrary reference frame can be written in the same manner,

$$v_{qs} = v_{qRs} + v_{qLs} \tag{2.14}$$

$$v_{ds} = v_{dRs} + v_{dLs} \tag{2.15}$$

$$v_{0s} = v_{0Rs} + v_{0Ls} \tag{2.16}$$

The voltage across stator resistor can be expressed as

$$v_{qRs} = r_s i_{qs} \tag{2.17}$$

$$v_{dRs} = r_s i_{ds} \tag{2.18}$$

$$v_{0Rs} = r_s i_{0s} \tag{2.19}$$

The voltage across inductive elements of stator circuit in arbitrary reference frame can be derived from equations (2.1) – (2.4)

$$v_{abcs} = p\psi_{abcs} \tag{2.20}$$

$$v_{qd0s} = K_s p\left[(K_s)^{-1}\psi_{qd0s}\right] \tag{2.21}$$

Equation (2.21) simplifies to

$$v_{qd0s} = \omega\psi_{dqs} + p\psi_{qd0s} \tag{2.22}$$

where,

$$\left(\psi_{dqs}\right)^T = \left[\psi_{ds} \; -\psi_{qs} \; 0\right] \tag{2.23}$$

where, ψ is the flux linkage and p is the differentiation operator.

By combining equations (2.14) - (2.19) and (2.22), the voltage equations of stationary three phase circuit in the arbitrary reference frame can be obtained as

$$v_{qs} = r_s i_{qs} + \omega\psi_{ds} + p\psi_{qs} \tag{2.24}$$

$$v_{ds} = r_s i_{ds} - \omega\psi_{qs} + p\psi_{ds} \tag{2.25}$$

$$v_{0s} = r_s i_{0s} + p\psi_{0s} \tag{2.26}$$

Similarly, voltage equations of rotor circuit in arbitrary reference frame can be expressed as

$$v_{qr} = r_r i_{qr} + \omega\psi_{dr} + p\psi_{qr} \tag{2.27}$$

$$v_{dr} = r_r i_{dr} - \omega\psi_{qr} + p\psi_{dr} \tag{2.28}$$

$$v_{0r} = r_r i_{0r} + p\psi_{0r} \tag{2.29}$$

There are several other reference frames, which are commonly used in electrical machines and power systems analysis such as stationary, rotor, and synchronous reference frame. The voltage equations for each reference frame can be derived from the aforementioned arbitrary reference frame. Table 2.1 provides the information regarding the reference frame interpretation and the speed.

TABLE 2.1

Commonly Used Reference Frames

Name	Interpretation	Reference frame speed
Arbitrary	Circuit variables referred to the arbitrary reference frame	ω (can be any value)
Stationary	Circuit variables referred to the stationary reference frame	0
Synchronous	Circuit variables referred to the synchronously rotating reference frame	ω_e

Rotor	Circuit variables referred to a reference frame fixed in the rotor	ω_r

where ω_e is the synchronous electrical angular frequency and ω_r is the rotor angular frequency.

2.2.2 Two Axes Model

Three-phase symmetrical induction motor dynamical model in stationary reference frame has been used throughout this thesis. Transformation of variables to the stationary reference frame was developed by E. Clarke, thus it is also known as Clarke's transformation. The notations used in the derivation of the arbitrary reference frame f_q, f_d, and f_0 change to f_α, f_β, and f_0 in stationary reference frame [45, 46].

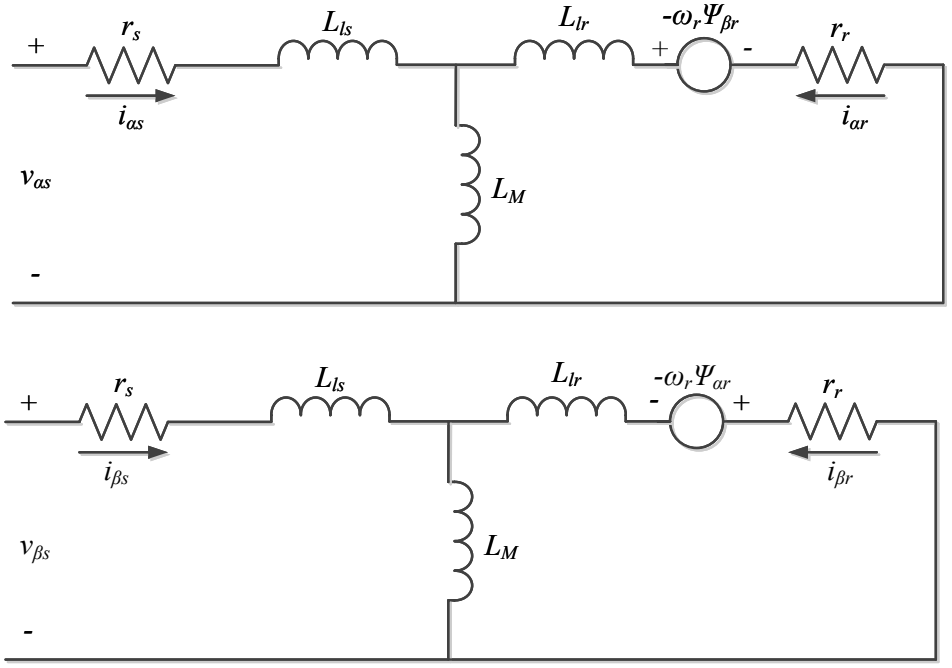

Fig. 2.3 Stationary reference frame equivalent circuit of three-phase symmetrical induction motor.

The mathematical model of the induction motor in the stationary reference frame, with direct axis attached to the stator phase 'a' which denoted by subscript 'α' and quadrature component denoted as subscript 'β' is given by [4].

$$\frac{d\psi_{\alpha s}}{dt} = -r_s i_{\alpha s} + v_{\alpha s} \tag{2.30}$$

$$\frac{d\psi_{\beta s}}{dt} = -r_s i_{\beta s} + v_{\beta s} \tag{2.31}$$

$$\frac{d\psi_{\alpha r}}{dt} = -r_r i_{\alpha r} - \omega_r \psi_{\beta r} \tag{2.32}$$

$$\frac{d\psi_{\beta r}}{dt} = -r_r i_{\beta r} + \omega_r \psi_{\alpha r} \tag{2.33}$$

$$\frac{d\omega}{dt} = \frac{1}{J}\left[T_e - T_L\right] \tag{2.34}$$

$$\omega_r = n_p \omega \tag{2.35}$$

where, ψ, i, v, ω and ω_r denoted the flux linkage, current, applied voltage components, mechanical speed and rotor electrical angular speed respectively. Subscripts *s* and *r* stand for stator and rotor components. r_s and r_r are the stator and rotor resistances and n_p is the number of pole pairs while J is the inertia of the motor. T_e and T_L denote electromagnetic torque and load torque respectively. The magnitude of the generated electromagnetic torque can be obtained as,

$$T_e = \frac{3}{2} n_p \frac{L_m}{L_r L_s'} \left|\underline{\psi}_r\right| \left|\underline{\psi}_s\right| \sin(\gamma) \tag{2.36}$$

where, $L_s' = L_s L_r - L_m^2$, γ is the angle between stator and rotor flux vectors , L_r and L_s are the rotor and stator inductance respectively and L_m is the mutual inductance. The relationship between flux and currents can be approximated by linear equations as follows. This is done without considering the magnetic saturation.

$$\underline{\psi}_s = L_s \underline{i}_s + L_m \underline{i}_r \tag{2.37}$$

$$\underline{\psi}_r = L_r \underline{i}_r + L_m \underline{i}_r \tag{2.38}$$

Stator and rotor direct and quadrature component currents in terms of stator flux components and the inductances can be obtained as,

$$i_{\alpha s} = \frac{L_r}{L_s'} \psi_{\alpha s} - \frac{L_m}{L_s'} \psi_{\alpha r} \tag{2.39}$$

$$i_{\beta s} = \frac{L_s}{L'_s}\psi_{\beta s} - \frac{L_m}{L'_s}\psi_{\beta r} \tag{2.40}$$

$$i_{\alpha r} = \frac{L_s}{L'_s}\psi_{\alpha r} - \frac{L_m}{L'_s}\psi_{\alpha s} \tag{2.41}$$

$$i_{\beta r} = \frac{L_s}{L'_s}\psi_{\beta r} - \frac{L_m}{L'_s}\psi_{\beta s} \tag{2.42}$$

CHAPTER III

CONTROL OF INDUCTION MOTOR DRIVES

3.1 Introduction

Over the past decades, numerous control strategies have been developed for IM control to ensure high precision and less complexity. Most of the previous developments were built using the fundamentals of electric machine theories and classical control theories. Fig. 3.1 illustrates the basic structure of a typical induction motor control system which composed of the controller, inverter, sensors, the induction motor, and the load [11].

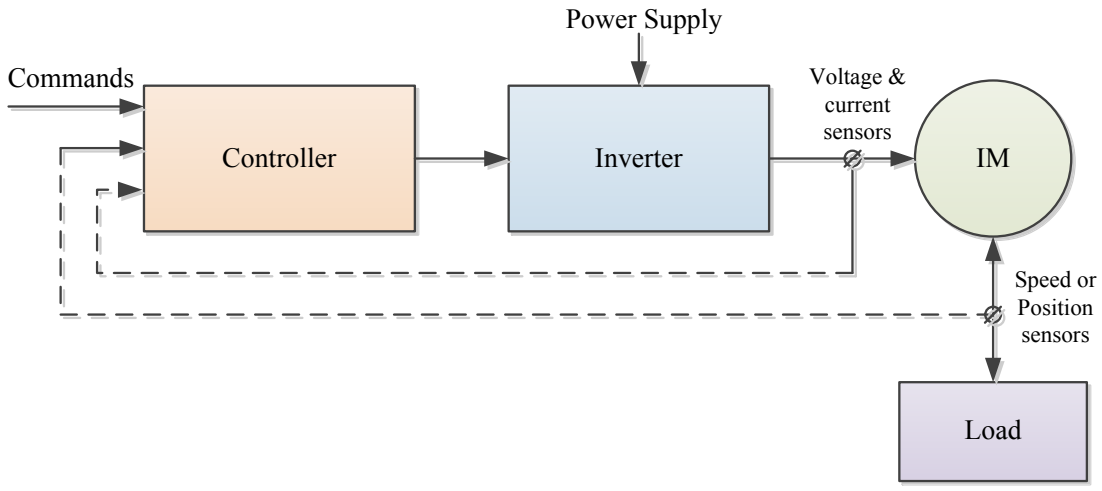

Fig. 3.1. Control system of an induction motor.

According to [47] an induction motor operation can be characterized by a fifth order nonlinear differential equations with three inputs and two state variables which are measurable. Machine parameter uncertainties and random disturbances further complicate the induction motor control systems. Nevertheless, there is a vast number

of control techniques available for induction motor control and new strategies continue emerging.

In this chapter, the fundamental theory behind the conventional direct torque control (CDTC) principle and two other nonlinear control mechanisms: sliding mode, and fuzzy logic control are discussed. Next, the sliding mode and fuzzy logic methods are combined with the proposed direct torque control mechanism.

3.2 Conventional Direct Torque Control

3.2.1 Direct Torque Control Basis

The principle behind the DTC method is to independently control the estimated torque and flux of the machine, using optimum switching vector table. Unlike in vector control, DTC does not control the flux and the torque of the motor by controlling the motor current. The direct torque control method also differs from vector control in a way, that it employs the stator flux instead of the rotor flux as in the vector control. Direct vector control and direct self control are two other variations of the DTC scheme.

3.2.2 Conventional Direct Torque Control Topology

The basic idea behind the DTC concept is to achieve decoupled control of both flux and torque by properly selecting the stator voltage analogous to the torque and flux errors. A block diagram of CDTC based induction motor drive is shown in Fig. 3.2 [20].

As depicted in the Fig. 3.2, a CDTC drive comprised of mainly four modules: an estimation block, a flux controller, a torque controller and the switching logic.

For the DTC scheme, estimated stator flux can be derived from (2.28) and (2.29) as,

$$\hat{\psi}_{\alpha s} = \int (\ \hat{v}_{\alpha s} - \ r_s \hat{\imath}_{\alpha s})\ dt \tag{3.1}$$

$$\hat{\psi}_{\beta s} = \int (\ \hat{v}_{\beta s} - \ r_s \hat{\imath}_{\beta s})\ dt \tag{3.2}$$

$$\hat{\psi}_s = \sqrt{\left(\hat{\psi}_{\alpha s}\right)^2 + \left(\hat{\psi}_{\beta s}\right)^2} \tag{3.3}$$

$$\hat{\theta}_{\psi s} = \tan^{-1}\left[\frac{\hat{\psi}_{\beta s}}{\hat{\psi}_{\alpha s}}\right] \tag{3.4}$$

The electromagnetic torque can be estimated as,

$$\hat{T}_e = \frac{3}{2} n_p \left(\hat{\psi}_{\alpha s}\hat{\imath}_{\beta s} - \hat{\psi}_{\beta s}\hat{\imath}_{\alpha s}\right) \tag{3.5}$$

Where $\hat{\theta}_{\psi s}$ is the stator flux angle.

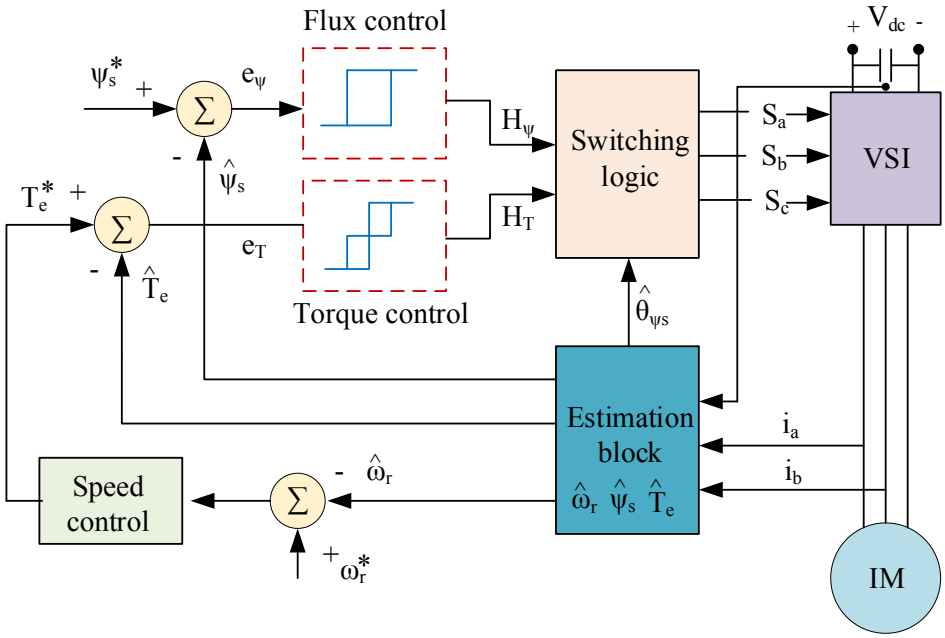

Fig. 3.2. Control structure of the CDTC

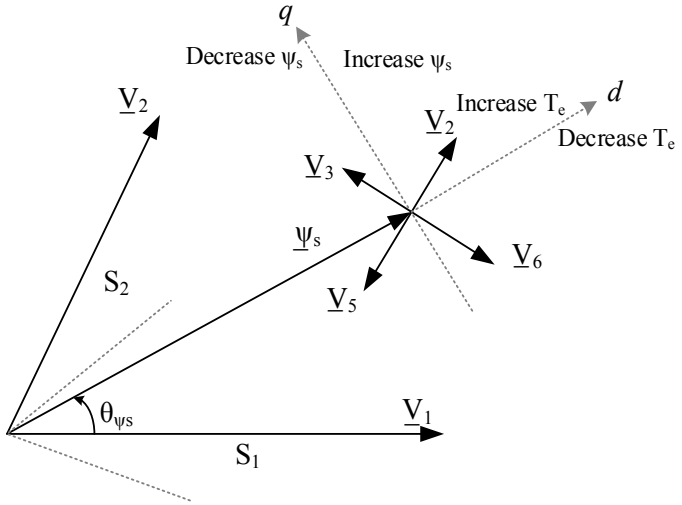

Fig. 3.3. Control principle of the CDTC in complex plane

In Fig. 3.3, V_i for $i = \{0,1, \dots ,6\}$ denotes the active voltage vectors and S_x for $x = \{1,2\}$ represents the first two sectors in complex plane. The estimated stator flux and torque values are calculated according to (3.3) and (3.5) are compared with their corresponding reference values ψ_s^* and T_e^* respectively. As illustrated in Fig. 3.2, the error between T_e^* and $\hat{T}_e$ is the input of a three-level hysteresis controller used in torque control loop. The error between ψ_s^* and $\hat{\psi}_s$ is the input of a two-level hysteresis controller which is used in stator flux control loop. Outputs from the two-hysteresis controllers together with the stator flux sector are used to select switching logic in CDTC method as described in the Fig. 3.3.

3.3 Sliding Mode Control

Sliding mode control (SMC) is one of the most popular discontinuous feedback control methods which is been extensively explored by many authors in various applications [12, 14, 26]. SMC has gained its popularity in the field of the nonlinear control system, due to its low sensitivity for the model parameter variation and disturbance as well as its order reduction property. SMC can also be treated as an extension of the classical hysteresis control, with the advantage of strict stability [14] which has been extensively considered in this study. In this section, the basic theory behind the sliding mode concept is discussed.

3.3.1 General Theory

The complete sliding mode operation can be divided into two stages [29]. The first stage is known as the reaching phase in where, SMC directs the control trajectory toward the sliding manifold, or sliding surface ($\zeta = 0$) regardless of the initial conditions. The second stage of the control process, which is known as sliding phase, starts as the trajectory reaches the sliding manifold. Thereafter, the control action ensures that the trajectory stays on the sliding surface, and simultaneously directed toward the required equilibrium point. The control method employs the sliding surface as the reference path and SMC makes the control trajectory to follow the reference path and ultimately reach the steady-state. The graphical representation of the control trajectory with SMC is illustrated in Fig. 3.4.

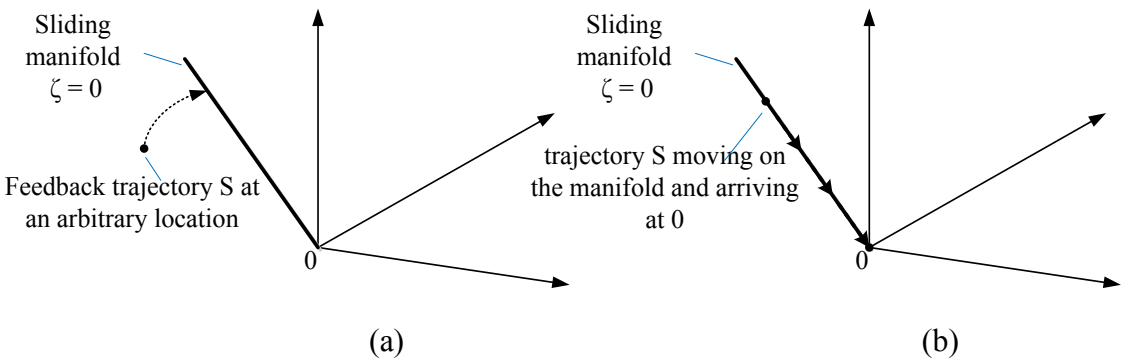

Fig. 3.4. Sliding mode control for ideal case [29] (a) Reaching phase (b) Sliding phase

Fig. 3.4 shows the behavior of the control trajectory for sliding mode process under ideal condition. Nonideality of the switching affects during the sliding phase and causes the trajectory to oscillate around the sliding manifold while simultaneously reaching toward the equilibrium point at 0. In addition, once it reaches equilibrium, the trajectory may become trapped in a periodically oscillating state as shown in Fig. 3.5 [29].

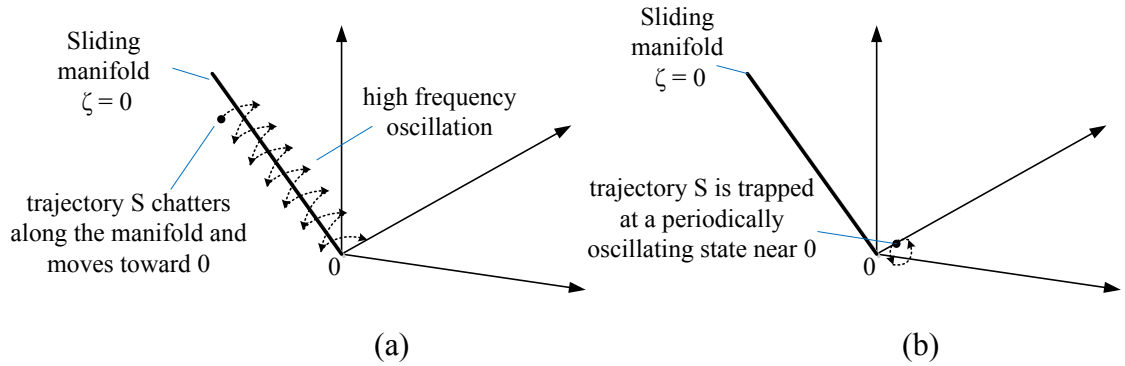

Fig. 3.5. Sliding mode control for non-ideal case [29] (a) Sliding phase (b) Steady state

3.3.2 Mathematical Formulation

A non-linear, time varying switching system can be defined as [29]

$$\dot{x}(t) = g\big(x(t)\big) + \varphi\big(x(t)\big)u(t) \tag{3.6}$$

where, $x(t)$ is state vector with n-dimension, $g(.)$ and $\varphi(.)$ are two vector fields in the same space, and the discontinues control function $u(t)$ can be expressed as

$$u(t) = \begin{cases} U^+ & if\ S(x,t) > 0 \\ U^- & if\ S(x,t) < 0 \end{cases} \tag{3.7}$$

where U^+ and U^- can be either constant values or functions of $x(t)$ and $S(x,t)$ is the instantaneous control trajectory.

A system with aforementioned structure needs to meet three conditions to exhibit sliding mode property, namely hitting, existence and stability conditions. The intention of the hitting condition is to guarantee that the control trajectory reaches the sliding manifold regardless of the initial condition. The necessary and sufficient condition for a system to satisfy the hitting condition is that the control action $u(t)$ must generate state-vector $x(t)$ and as result control trajectory should satisfy the following inequality [14, 29],

$$S\frac{dS}{dt} < 0 \qquad (for\ t > 0\ and\ |S| \geq \delta) \tag{3.8}$$

where, $^{d}/_{dt}$ is the time derivative and δ is the width of the sliding surface.

The second criteria, which is the existence condition, ensures that the control trajectory near the sliding manifold such that $0 < |S| < \delta$, is always directed toward the sliding manifold. This can be validated by checking the local reachability condition of the equation (3.8) as [29],

$$\lim_{S \to 0} S\frac{dS}{dt} < 0 \tag{3.9}$$

The stability condition is used to ensure that the trajectory in the sliding manifold always directed toward the equilibrium steady state point. This is done by selecting the control action and the sliding coefficients to comply with stability criteria.

3.3.3 Hysteresis Function

The implementation of the sliding mode through hysteresis function is commonly used in control applications. Direct implementation of the sliding mode in control action creates problems such as high switching frequency and undesirable chattering problems. These problems can be avoided by employing hysteresis function to restrict the range of the switching frequency. The switching function in equation (3.7) can be redefined with the

incorporation of hysteresis concept as,

$$u(t) = \begin{cases} U^{+} & if\ S(x,t) > \Delta \\ U^{-} & if\ S(x,t) < -\Delta \\ Previous\ state & otherwise \end{cases} \tag{3.10}$$

where, Δ is an arbitrary value. With the introduction of hysteresis bandwidth of 2Δ, the control trajectory bounds in between ±Δ ensuring the controllable chattering as a function of Δ. Fig. 3.6 demonstrates the sliding mode operation through hysteresis function.

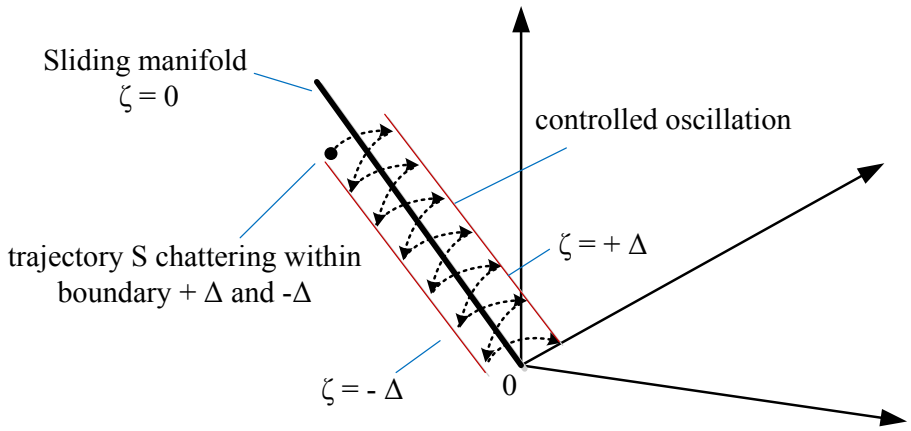

Fig. 3.6. SMC with hysteresis control

3.4 Fuzzy Logic Control

As discussed in section 3.2, DTC in its basic configuration employs two hysteresis controllers in torque and flux control loops. However, these hysteresis controllers create two major issues for DTC drives. They are: 1) variable switching frequency and 2) high torque ripple. These issues lower the performance and add losses to the drives. Numerous control approaches have been proposed in literature to overcome these problems associated with the CDTC drives [48, 49].

In this study, the adaptive nature of the fuzzy logic control (FLC) has been incorporated to enhance the dynamic performance of the DTC drive by replacing the hysteresis controllers with fuzzy logic based controllers. The proposed approach is discussed in chapter IV. This section is devoted to an exposition of the fundamental of the FLC

technique and its implications in the feedback regulation of the nonlinear systems.

3.4.1 Fuzzy Set

The notion of the fuzzy set is derived as an extension of the classical set theory. However, as in the classical set, the fuzzy set does not have a sharp boundary. It is an object in a classical set can either belong to a set or not belong to a set. Yet, an object in a fuzzy set can be categorized into more than one subset simultaneously, as its boundaries are smooth or vague. In other words, the fuzzy sets employ a universe of discourse as its base and take account of an infinite number of degrees of membership in a set. The universe of discourse is the range of all possible values for an input to a fuzzy system. Representation of classical and fuzzy set is shown in Fig. 3.7.

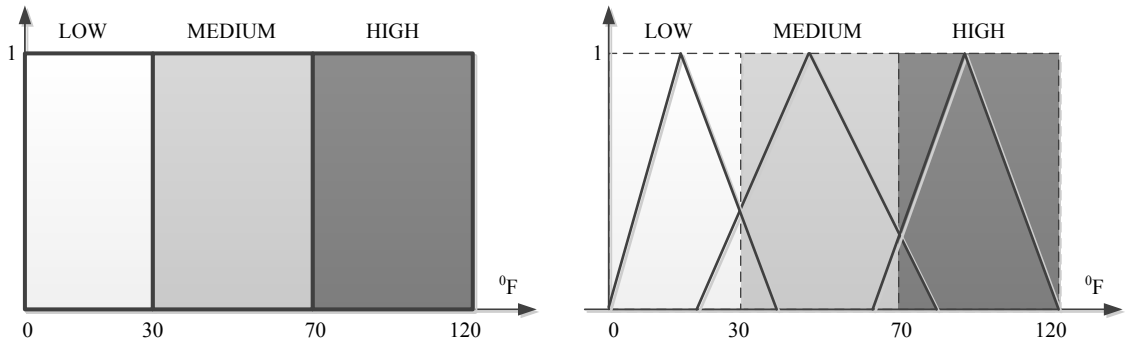

(a) (b)

Fig. 3.7. Illustration of set [50] (a) Classical (b) Fuzzy

Analogous to the classical set operations, the primary fuzzy set operations contain intersection, union and complement which can be defined as [50]

Union: $A \cup B = \mu_A(x) \cup \mu_B(x) = \max(\mu_A(x), \mu_B(x))$

Intersection: $A \cap B = \mu_A(x) \cap \mu_B(x) = \min(\mu_A(x), \mu_B(x))$

Complement: $A^c = F \backslash A$

where, A and B are two fuzzy sets, x is an element in the universe of discourse and μ is the membership function. The graphical representation of above fuzzy set operation is shown in Fig. 3.8.

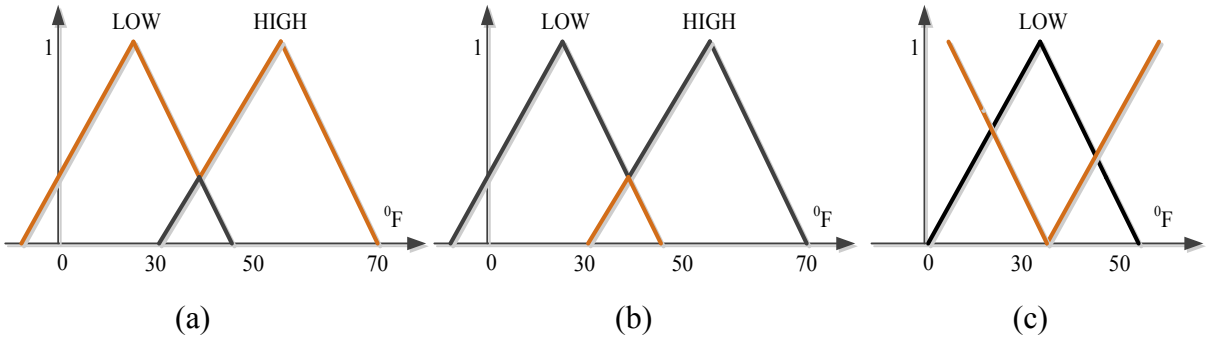

Fig. 3.8. Fuzzy set operation [50] (a) Union (b) Intersection (c) Complement

3.4.2 Fuzzy Inference System

In contrast to the standard control strategy, which is a point-to-point control, fuzzy logic control is a range-to-point or range-to-range control [50]. The process of formulating the mapping from a given input to an output using fuzzy logic is referred to as fuzzy inference [11]. The structure of a basic fuzzy inference system (FIS) is demonstrated in Fig. 3.9. A FIS generally comprises of three major sections namely, a fuzzifier, a fuzzy inference engine, a defuzzifier [33].

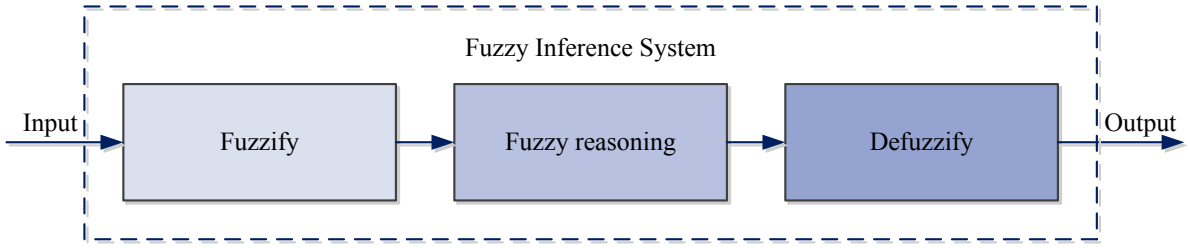

Fig. 3.9. A basic fuzzy inference system [11]

3.4.3 Fuzzification

Fuzzification is the first step in FIS. This involves converting crisp or classical variables into fuzzy variables and thereafter apply fuzzy inference procedures to obtain the desired output. Typically, fuzzification includes two steps, first generate membership function for input and output variables and carefully assign them with linguistic variables. This procedure is related to the mapping of a classical set to a fuzzy set with variable degrees.

In reality, there are several different types of membership functions, for instance triangular waveform, trapezoidal waveform, Gaussian waveform, bell-shaped waveform, sigmoidal waveform and S-curve waveform [50].The shape of the membership function is selected to match with the application requirements. The systems that require fast dynamic variation with smaller time laps, a triangular waveform is the best choice while a Gaussian or S-curve waveform is selected obtain precise control.

3.4.4 Fuzzy Rule Base

The second step of the FIS is to define control rules to create the control output. The control rules can be treated as the core of FIS. These rules are associated with the sequence of **if-then** conditions, generating an algorithm to express the series of action should be taken with respect to the current observations. 'If' part captures the information of the observed input and 'then' part employed to generate output conclusion.

3.4.5 Defussification

As the final step in FIS process, control action selected from the previous step should be converted from the linguistic variables back to crisp or classical variables, to use in the control objective. In practice, there are three defuzzification techniques are used Mean of Maximum method, Center of Gravity method and the Height method [50].

CHAPTER IV

METHODOLOGY

4.1 Sector Advancing Strategy

4.1.1 Overview of Sector Advancing Concept

Numerous developments of the basic DTC algorithm have been evolving over the past few years in order to enhance the dynamic performance and the efficiency of the motor drives as well as to improve the quality of stator current [4, 12, 21, 22, 24-26, 28, 34, 36, 43, 51-53]. As such, an interesting concept that is being used to improve the dynamic operations of DTC based induction motor drive is "sector advancing (SA)" which is also known as sector shifting [44]. This notion is employed in drives so that fast torque response can be achieved which is a key indicator of drive quality of dynamic performance.

The fundamental structure of the DTC algorithm with SA concept is similar to the CDTC method, which is illustrated in Fig. 3.2. However, the selection procedure of the voltage vector v_i for $i = \{0,1, \dots,6\}$ has been altered to incorporate the SA strategy [44]. In the conventional method, v_i is selected from the basic switching look-up table as given in Table 4.1, considering the feedback error of both estimated torque and flux.

4.1.2 Selection of Voltage Vector

In CDTC, at each sampling state the required voltage vector is selected based on the error between estimated and reference stator flux. However, in the SA strategy, the voltage vector selection process has been modified allowing induction machine to achieve fast torque response. The underlying principle behind the SA scheme is illustrated in this section.

If the rotor flux remains constant when stator flux is changed incrementally by applying stator voltage with corresponding variation of the angle γ ($\Delta\gamma$), then the incremental electromagnetic torque, ΔT_e can be derived as,

$$\Delta T_e = \frac{3}{2} n_p \frac{L_m}{L_r L_s'} \left|\underline{\psi}_r\right| \left|\underline{\psi}_s + \Delta\underline{\psi}_s\right| \sin(\Delta\gamma) \tag{4.1}$$

It can be seen that higher torque increment can be achieved by properly adjusting either $\Delta\underline{\psi}_s$ or $\Delta\gamma$. In this thesis, a rapid torque increment is obtained via $\Delta\gamma$, which is by changing the angle between the rotor and the stator flux vector rapidly, for a time increment of Δt.

Depending on the place where $\underline{\psi}_s$ lies, in one of the six sectors of the α-β reference frame, v_i has different influence for the stator flux and the electromagnetic torque. If a particular v_i in one sector of the complex plane is employed to increase the stator flux, the same voltage vector can be used to decrease the stator flux in the next sector. This idea is incorporated to develop a new switching control strategy with SA concept.

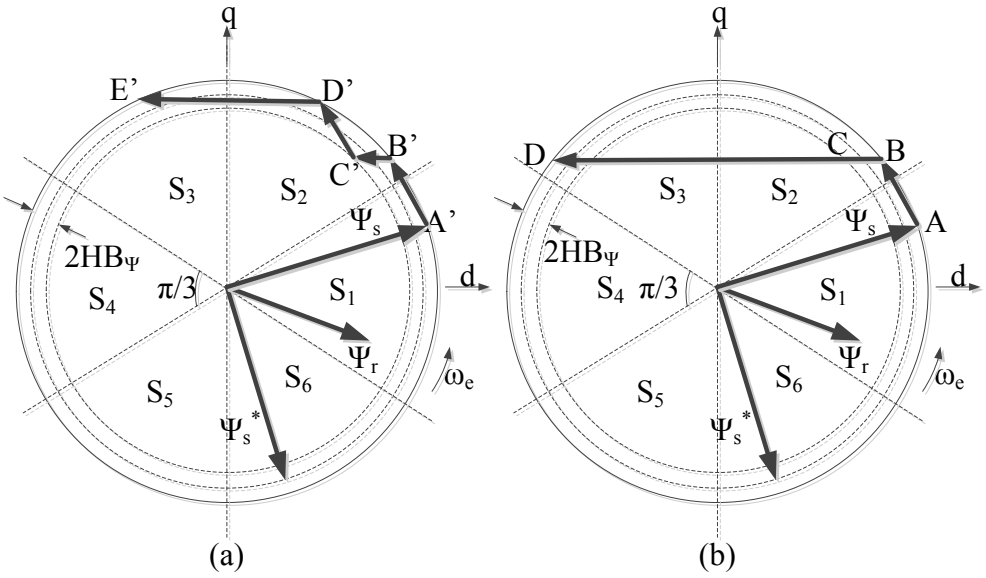

Fig. 4.1. Trajectories of stator flux vector (a) Conventional DTC (b) DTC with SA strategy [44, 54]

Consider, for example, an operation in sector 2 as depicted in Fig.4.1 (b) at point B, flux is high and torque is low, that is $H_\psi = -1$ and $H_{Te} = 1$. According to the switching strategy established in Table 4.1, voltage vector V_4 is applied to the drive in order to keep flux and torque within their hysteresis band, $2HB_\psi$, thus creating the trajectory up to

point C. Thereafter, at point C, $H_\psi = 1$ and $H_{Te} = 1$, that is both flux and torque need to be increased and this will generate V_3 from the Table 4.1, according to the conventional method as depicted in Fig. 4.1 (a) trajectory C'D'. However, in SA approach, instead of selecting V_3 from the look-up table, it makes flux space vector to function as it is in the sector 3. If the flux vector is at the sector 3, and feedback signals are $H_\psi = 1$ and $H_{Te} = 1$, then the voltage vector should be applied is V_4. Thus V_4 will apply until the flux vector touches the upper bound of the hysteresis controller as illustrated by trajectory CD in Fig. 4.1 (b). It can be observed that stator flux trajectory follows a different path in contrast to the ordinary trajectory described in Fig. 4.1 (a) which is bounded by the hysteresis bandwidth of $2HB_\psi$.

TABLE 4.1

Switching Strategy of Conventional DTC

H_ψ	H_{Te}	S_1	S_2	S_3	S_4	S_5	S_6
1	1	V_2	V_3	V_4	V_5	V_6	V_1
	0	V_0	V_7	V_0	V_7	V_0	V_7
	-1	V_6	V_1	V_2	V_3	V_4	V_5
-1	1	V_3	V_4	V_5	V_6	V_1	V_2
	0	V_7	V_0	V_7	V_0	V_7	V_0
	-1	V_5	V_6	V_1	V_2	V_3	V_4

In CDTC the stator flux vector travels along the circular trajectory at a constant speed determined by the applied DC voltage of the voltage source inverter. However, with the SA technique the stator flux vector follows a shortcut path and reaches the next location within a shorter time compared to the original locus. Flux vector trajectory following a different path yields a sudden increment of the angle between the stator and rotor flux vectors and rapid torque increment. This concept, which is used to separate the stator flux vector from rotor flux vector in larger angle, is referred to as sector advancing. In this research, the SA technique [44] is applied to the CDTC algorithm together with the proposed fuzzy logic and sliding mode control methods to get better dynamic

performance from the drive.

In Fig. 4.1, d and q represent the direct and quadrature axes in complex plane while ω_e is the angular frequency of the stator flux. In Table 4.1, H_ψ and H_{Te} represent levels of digital outputs of flux and torque control loops. S_i for $i = \{0,1, \dots ,6\}$ represents the sector number.

4.2 Proposed Control Algorithms for DTC

In this section, complete design procedure of SM and FL based torque and stator flux controllers are described. These two algorithms are combined with the SA algorithm discussed in section 4.1.

4.2.1 Sliding Mode in DTC

SMC is used to achieve a robust and fast dynamic performance for IM drive. SMC enforces the system to stay on the pre-defined sliding surface by adaptively adjusting the structure of the controller. Fig. 4.2 shows the proposed integral type sliding mode DTC (SMDTC) scheme. The drive employs a proportional-integral (PI) speed controller, stator flux, torque and speed observers. The control objective of the drive is to control the stator flux magnitude and the torque of the machine.

The controllers are constructed to enforce the stator flux and torque to follow their command values. The sliding surfaces for stator flux magnitude and electromagnetic torque are designed to impose SM operation with first order dynamics. We define the sliding surfaces as $S_{\psi s}$ for the flux controller and S_{Te} for torque controller as

$$S_{\psi s} = e_{\Psi \mathrm{s}} + k_{\Psi \mathrm{s}} \int e_{\Psi \mathrm{s}}\, dt \tag{4.2}$$

$$S_{Te} = e_{\mathrm{Te}} + k_{\mathrm{Te}} \int e_{\mathrm{Te}}\, dt \tag{4.3}$$

$e_{\psi s} = \psi_s^* - \hat{\psi}_s$ is stator flux error, $e_{Te} = T_e^* - \hat{T}_e$ is torque error, $k_{\Psi \mathrm{s}}$ and k_{Te} are design constants. The control laws are selected such that system states to stay on the surfaces $S_{\psi s} = 0$ and $S_{Te} = 0$ [12]. First order linear dynamics of the stator flux error and torque error are given by

$$\frac{de_{\psi s}}{dt} = -k_{\psi s} e_{\psi s} \tag{4.4}$$

$$\frac{de_{Te}}{dt} = -k_{Te}e_{Te} \tag{4.5}$$

In this case, the design constants are chosen to have desired dynamics for the control errors. Then, the switching controls for the flux and torque controllers can be written as

$$u_{\psi s} = U_0 sgn(S_{\psi s}) \tag{4.6}$$

$$u_{Te} = U_1 sgn(S_{Te}) \tag{4.7}$$

The constants U_0 and U_1 are derived from the Lyapunov stability condition as in (53) and (54) [35].

$$S_{\psi s}\dot{S}_{\psi s} < 0 \tag{4.8}$$

$$S_{Te}\dot{S}_{Te} < 0 \tag{4.9}$$

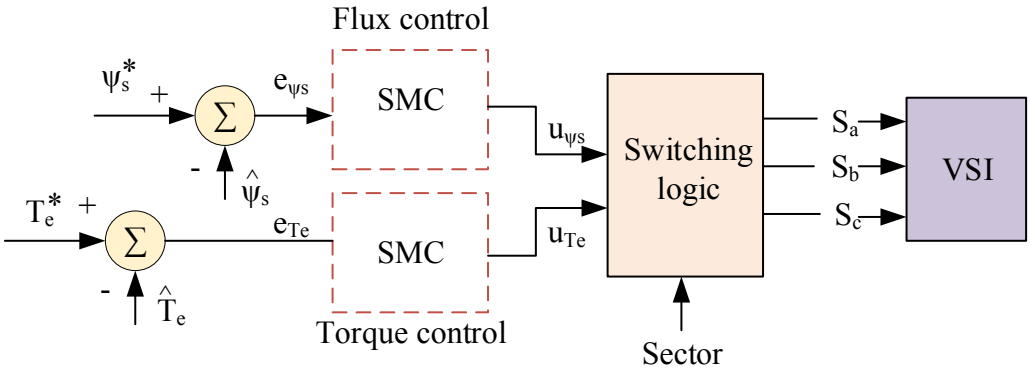

Fig. 4.2. SM based control scheme for DTC

Switching signals $u_{\psi s}$ and u_{Te} are used to select proper voltage vector for the Voltage Source Inverter (VSI).

4.2.2 Fuzzy Logic in DTC

Integration of intelligent control techniques, including fuzzy logic, neural networks, and genetic algorithm is becoming more popular along with the rapid development of the power electronics. This thesis deploys a fuzzy logic strategy to improve the dynamic as well as steady-state performance of the DTC drives. In conventional DTC, the higher ripples in torque and flux pose a real problem for IM drive applications. In this section, the proposed FL approach is employed to reduce the inherent problem in CDTC. The target is achieved by replacing the hysteresis controllers in classical method with two

FLCs, one in stator flux control loop and the other one in electromagnetic torque control as depicted in Fig. 4.3.

In order to obtain better performance, two PI type FLCs are introduced in both flux and torque control loops. Compared to the traditional PI type controller, a FL based PI controller has lower steady state error. In this approach, fuzzy controllers are designed to have one input and two outputs separately as shown in Fig. 4.3.

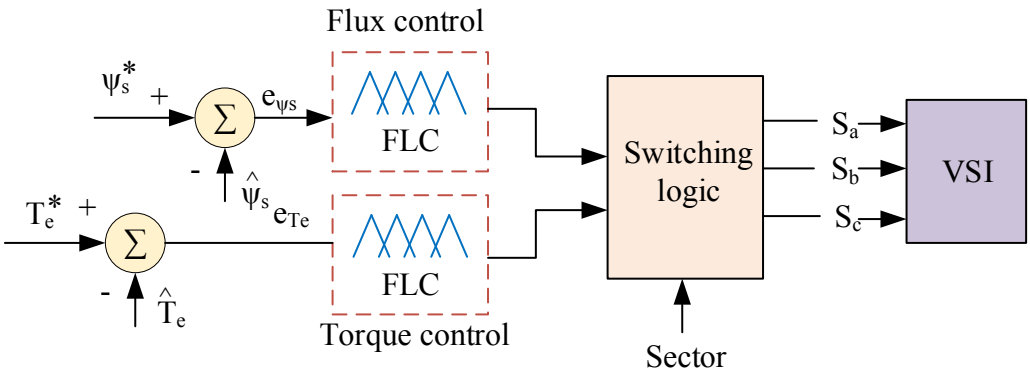

Fig. 4.3. FL based control scheme for DTC

In traditional PI controller, proportional gain K_p and integral gain K_i are constant. In the proposed approach, these gains are varied in accordance with the error to enhance the better performance of the controller. This has been achieved by varying μ_p and μ_i which are based on the defined fuzzy rules. The percentage variation of μ_p and μ_i are determined by the absolute value of the error between command values (T_e^* and ψ_s^*) and the estimated values ($\hat{T}_e$ and $\hat{\psi}_s$) during the operation. Then, the K_p and K_i for FL based PI controller can be defined as

$$K_p = W_{k_p}\mu_p \tag{4.10}$$

$$K_i = W_{k_i}\mu_i \tag{4.11}$$

where, W_{k_i} and W_{k_p} are the weighting factors.

Similar structure is used for both stator flux and torque control loops. In stator flux control loop, the absolute value of the error between command stator flux, ψ_s^* and the estimated stator flux, $\hat{\psi}_s$ is taken as the input. Two gain values are placed in the controller

loop where, μ_p and μ_i are the two outputs of the fuzzy controller. The absolute error between reference torque, T_e^* and the estimated torque, $\hat{T}_e$ is used as the input to the fuzzy torque controller. The controller produces the corresponding gain values based on the defined fuzzy rules.

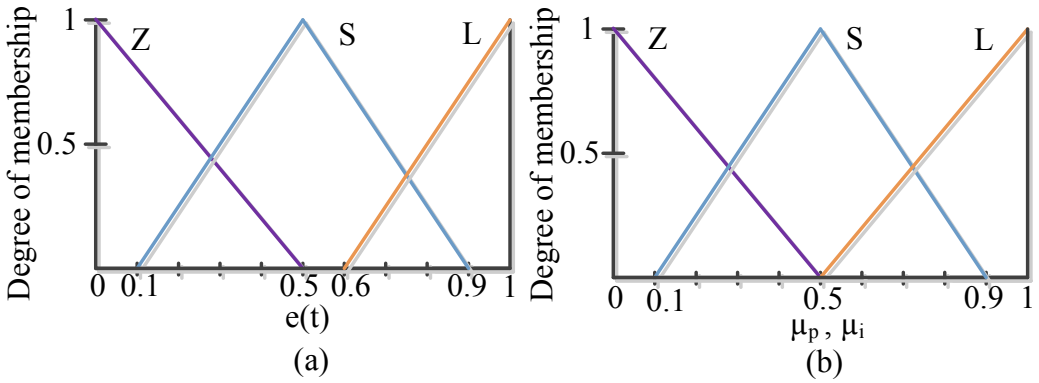

Fig. 4.4. Fuzzy membership functions (a) Input error (b) Output gains, μ_p and μ_i

Designed MFs of the two controllers are shown in Fig. 4.4. Triangular MFs are used except at the extreme ends. The fuzzy inference rules used for the controllers are defined as in [11, 33]

Rule 1: if abs $e(t)$ =L then μ_p= L and μ_i = L

Rule 2: if abs $e(t)$ =S then μ_p= L and μ_i = Z

Rule 3: if abs $e(t)$ =Z then μ_p= L and μ_i = S

Where $e(t)$ is torque or stator flux error, L for large, S for small and Z for zero. Input of the controller maps to the two outputs based on the defined rule base. The gains of the controller are adjusted adaptively considering the absolute value of the $e(t)$. Finally, the outputs of the torque and flux control loop together with sector number are used to obtain the best voltage vector for VSI.

CHAPTER V

SIMULATION RESULTS

Computer simulation is a powerful tool for analyzing an induction motor control system. In computer simulation environment, all the parameters and states of the model can be readily observed, and parameters can be changed easily to understand the effect on the model, thereby permitting a flexible design of the control system. This chapter is mainly composed of two parts. In the first section, characteristics of the three phase symmetrical induction motor in the stationary reference frame are described. The latter part presents the analysis of the proposed method by comparing the different techniques and various test cases.

5.1 Induction Motor Modeling

In order to demonstrate the transient behavior of the three phase induction motor, a simulation study of direct on-line starting was carried out. At the initial time instant (i.e. t = 0s), the motor is at standstill. The motor is powered by 220V, 60 Hz three phase supply and the amplitude of each phase voltage equals to $\sqrt{2} \times \left({}^{220}/_{\sqrt{3}}\right) = 179.63\ V$. The parameters of the three phase induction motor used for the simulation are given in the Appendix. Motor transient operation under free acceleration and with a load are discussed.

5.1.1 Induction Motor Operation under Free Acceleration

It is important to examine the behavior of the induction machine variables during no load acceleration period to steady state operating point. Hence, the nonlinear differential

equations given in Chapter II which describes the characteristics of the symmetrical induction machine, are simulated and results are presented.

The three phase stator voltage components, v_a, v_b, and v_c are showed in Fig. 5.1. Each phase voltage has a peak magnitude, V_m equals to 179.63V and contains $\mp 120^0$ phase shift with respect to phase 'a'. Fig. 5.2 shows the stator voltage in the stationary reference frame. Three phase voltage components have been transformed into two perpendicular voltage components such that

$$V_m = {}^{2}/_{3}\sqrt{(v_{\alpha s})^2 + \left(v_{\beta s}\right)^2} \tag{5.1}$$

Where $v_{\alpha s}$ and $v_{\beta s}$ are the stator voltage components in two axes reference frame. Startup transient of the stator voltage in the stationary reference frame is illustrated in Fig. 5.3. Where, $i_{\alpha s}$ and $i_{\beta s}$ represent the direct and the quadrature components of the stator current.

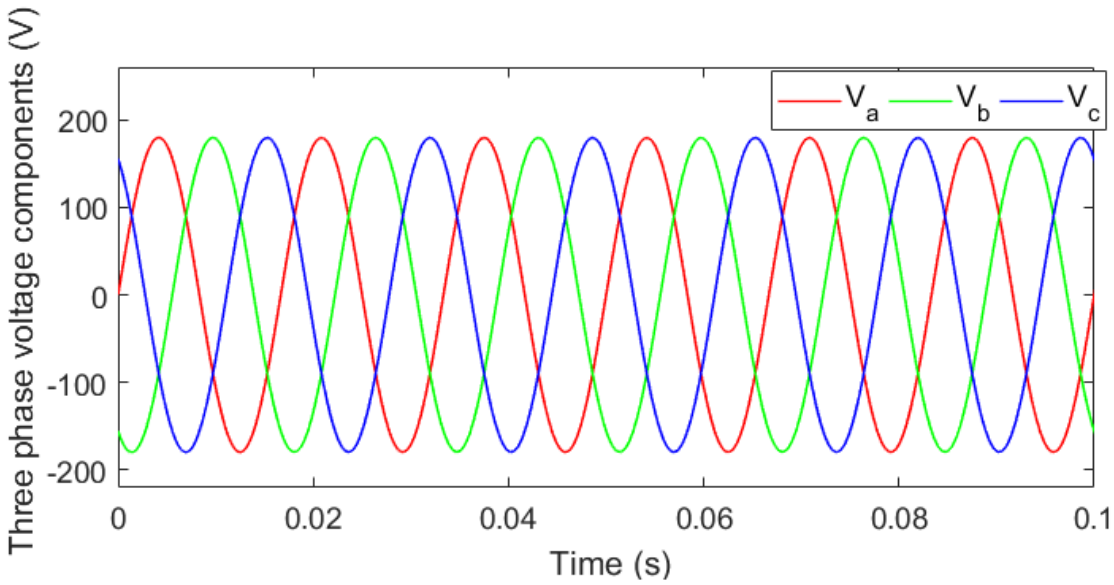

Fig. 5.1. Three phase components of the stator voltage.

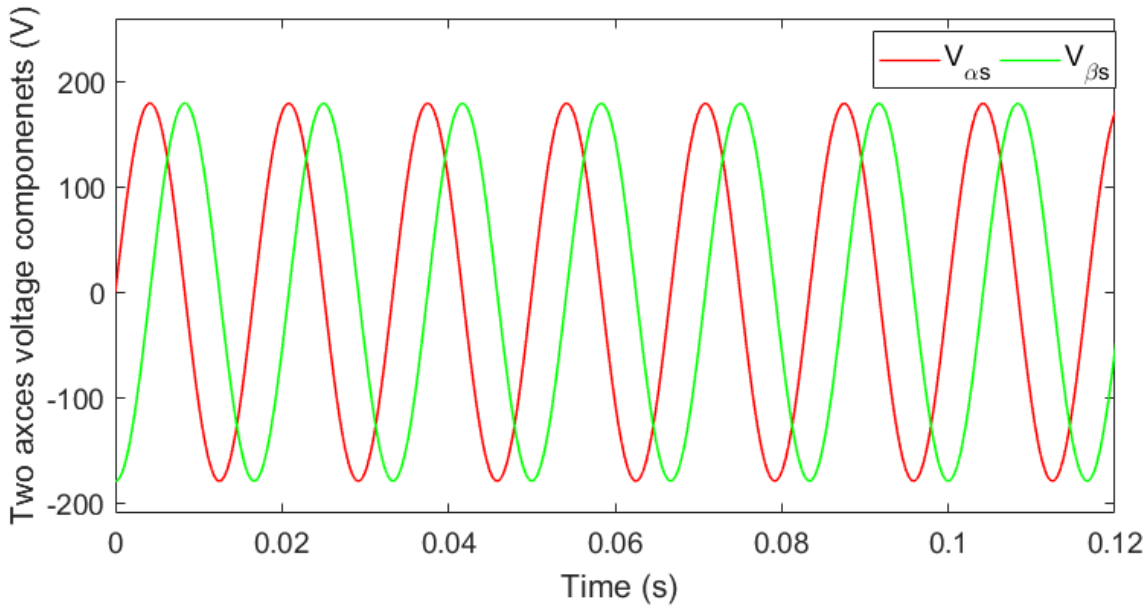

Fig. 5.2. Two axes components of the stator voltage.

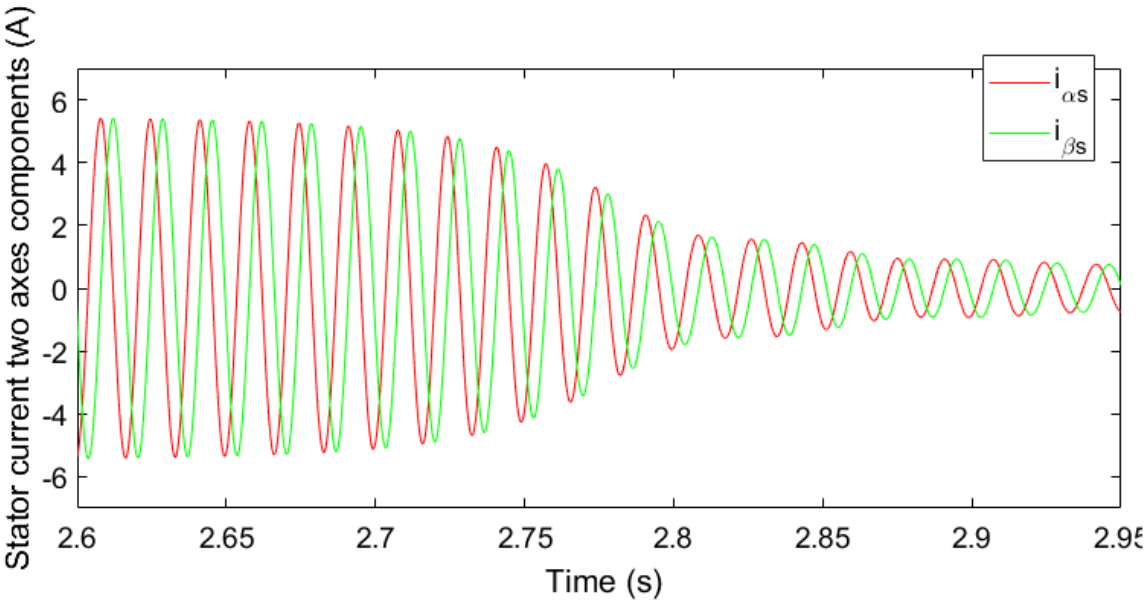

Fig. 5.3. Two axes components of the stator current.

Fig. 5.4 and Fig. 5.5 represent the rotor speed and the electromagnetic torque generated by the induction machine during free acceleration from the stall. As observed from the Fig. 5.4, the motor takes 3s to reach the steady state speed of 188.5 rad/s (1800 rpm).

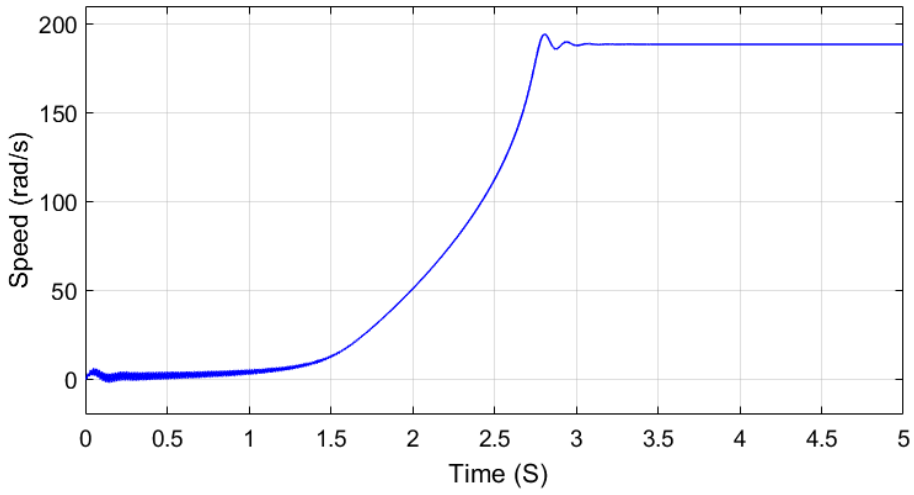

Fig. 5.4. Rotor speed variation under no-load.

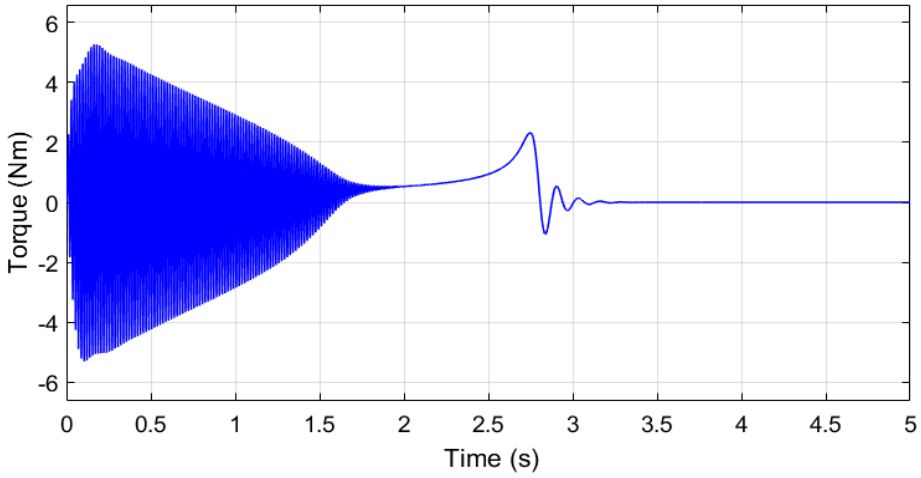

Fig. 5.5. Electromagnetic torque variation of the motor under no-load.

5.1.2 Induction Motor Operation under a Load

It is essential to analyze the motor performance when a load is connected. For this purpose, a constant load torque of 3 Nm is applied to the motor at t = 4s. Corresponding responses of stator current, rotor speed, and motor torque are demonstrated in Fig. 5.6 – Fig. 5.8. The stator phase 'a' current variation during initial transient and the load application are shown in Fig. 5.6. It can be seen that a three phase induction motor draws a higher current during starting when operated at direct on line start. In practice, this is avoided by controlling the induction motor through a high performance variable speed

drive (VFD). These VFD devices consist of power electronics semiconductor switching devices which can generate desired output characteristics based on switching control.

Fig. 5.7 shows the rotor speed response with a load connected. It can be noticed that, initially the motor spins at the synchronous speed. When the load torque is stepped from zero to the given value, the speed of the motor drops to 182.3 rad/s (1740.8 rpm) due to the slip. Dynamic behavior of the electromagnetic torque during a step change in load torque is shown in Fig. 5.8. Motor electromagnetic torque reaches the desired load torque after undergoing slight fluctuations.

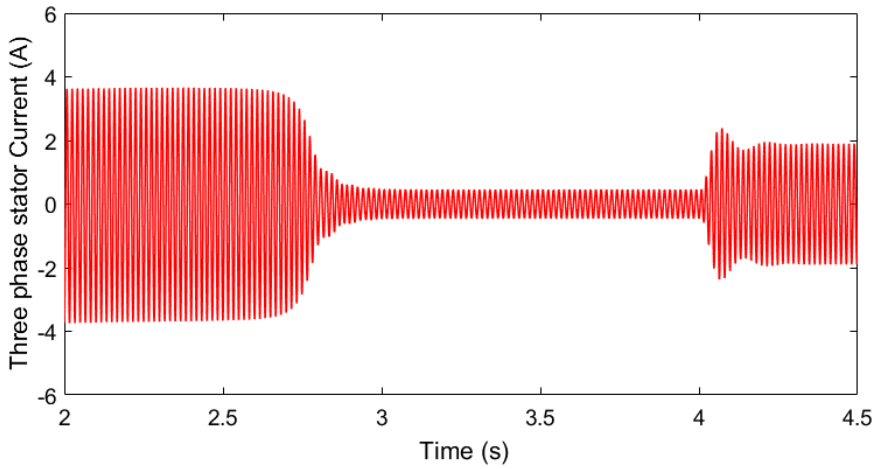

Fig. 5.6. Stator current phase ‘a’ variation under loaded condition.

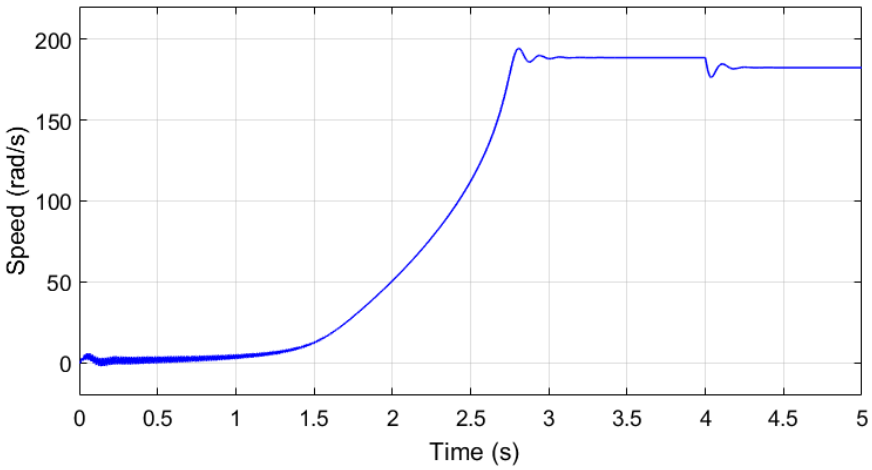

Fig. 5.7. Rotor speed variation under loaded condition.

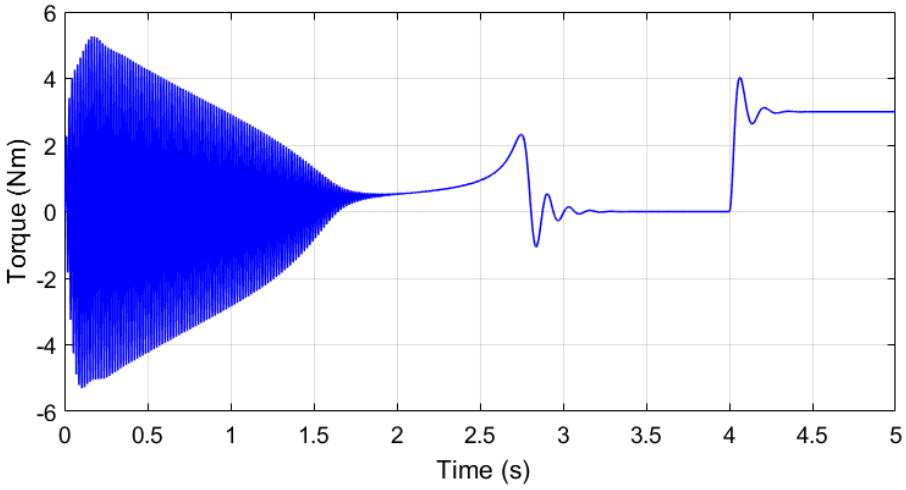

Fig. 5.8. Electromagnetic torque variation of the motor under loaded condition.

5.2 Proposed Approach for DTC Drives

The proposed DTC approach together with FL and SM control techniques were simulated in Matlab/ Simulink environment. Three-phase induction motor parameters which have been used for the simulation are given in the Appendix. A PI controller has been utilized in speed control loop, which generates the electromagnetic torque reference (T_e^*) for the DTC scheme. The speed controller gains were chosen as, $k_p = 3$, $k_i = 0.001$. Speed and stator flux reference values used in the entire simulation were 100 rad/s and 0.8 Wb respectively. A step change to the speed controller reference was applied at t = 0.2s. The performance and the effectiveness of the proposed DTC algorithm are evaluated through a series of test cases.

5.2.1 Startup Transient

The behaviors of each control method subjected to a load connection are examined in this section. A constant load torque of 6 Nm is applied at 0.65s to each motor, driven by different control strategies. The torque response, speed response and the stator flux locus of CDTC without SA, CDTC with SA, SMDTC with SA, and FLDTC with SA are demonstrated in Fig. 5.9 - Fig. 5.11.

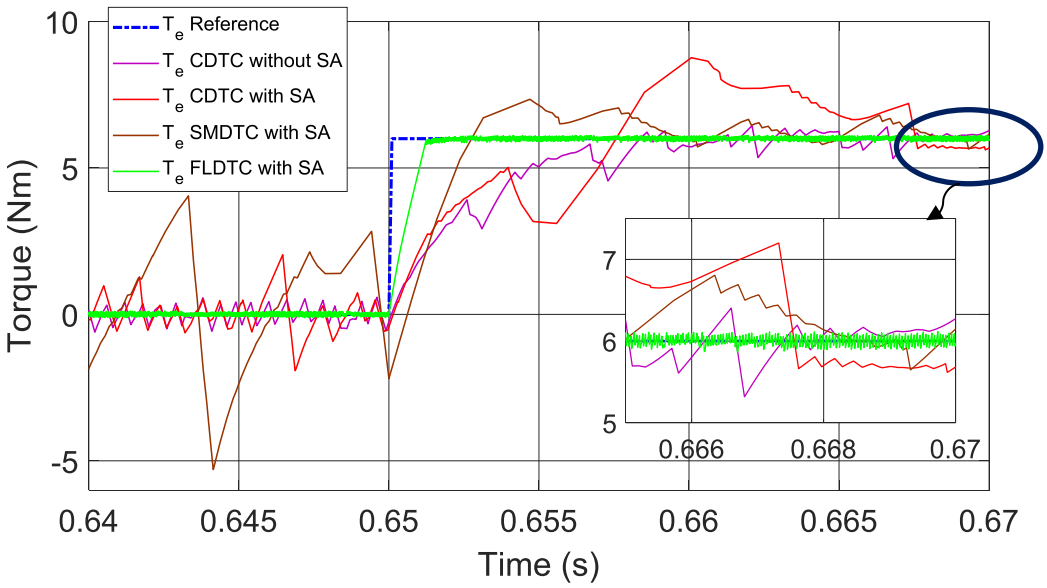

Fig. 5.9. Electromagnetic torque response during load application.

Fig. 5.9 shows the torque response during initial load application with the steady state zoom in view. Each controller illustrates different transient times during initial operation as depicted in Fig. 5.9. The torque response trajectory corresponds to the CDTC without SA takes 0.665s to reach the reference value. On the other hand, proposed controllers designed with SA scheme, with three different control methods, i.e. CDTC, SMDTC, and FLDTC take 0.658s, 0.653s and 0.651s respectively to reach the reference value.

When compared to CDTC without SA, the controllers that have been constructed with SA strategy display faster response for the electromagnetic torque on the expense of increasing the steady state chattering. Nevertheless, the chattering problem related with the conventional and SM based controllers has been fixed by the FLDTC due to its adaptive nature, while preserving the merits of the SA technique.

Fig. 5.10 depicts the speed regulation of designed controllers. Each controller follows the desired speed of 100 rad/s which was applied at t = 0.2s. The time taken to reach the steady state value varies depending on the available acceleration torque. As shown in Fig. 5.10, speed transient times and steady state speeds of CDTC without SA, CDTC with SA, SMDTC with SA and FLDTC with SA, are 0.39s; 99.7 rad/s, 0.43s; 100.1 rad/s, 0.42s; 100.1 rad/s and 0.4s; 100.03 rad/s.

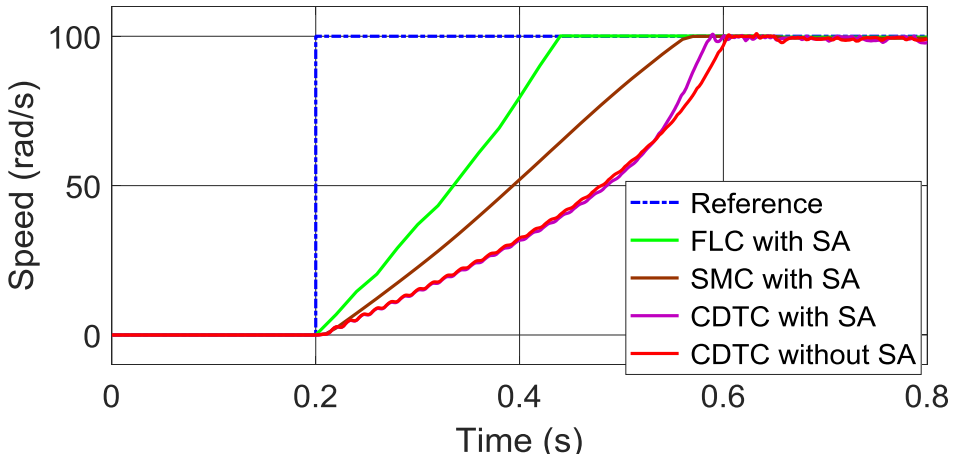

Fig. 5.10. Startup transient of the motor speed responses of different controllers

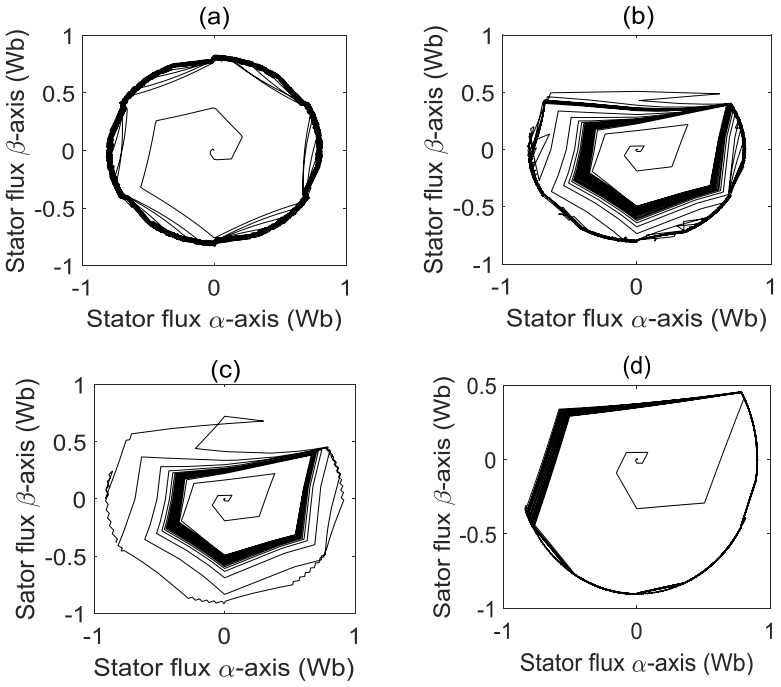

Fig. 5.11. Stator flux trajectory. (a) CDTC without SA (b) CDTC with SA (c) SMDTC with SA (d) FLDTC with SA.

The locus described by the extremity of the stator flux vector in complex plane is demonstrated in Fig. 5.11. The stator flux trajectory of the CDTC without SA is almost circular as shown in Fig. 5.11 (a). The stator flux locus of the controllers that are designed with SA strategy are shown in Fig. 5.11 (b) – Fig. 5.11 (d). Stator flux trajectories of the controllers designed with SA do not resemble a circle. This is due to

the different voltage vector selection strategy employed in SA approach when compared to the traditional look-up table method. In order to obtain a fast torque response, the angle between stator flux and the rotor flux is increased rapidly permitting the flux vector to follow a different path. Therefore, Fig. 5.11 (b) – Fig. 5.11 (d) have considerably similar loci that resulted from SA method. Fig. 5.12 shows the variation of the stator voltage components of FLDTC. During initial transient and steady state periods, the nature of the stator voltage is different.

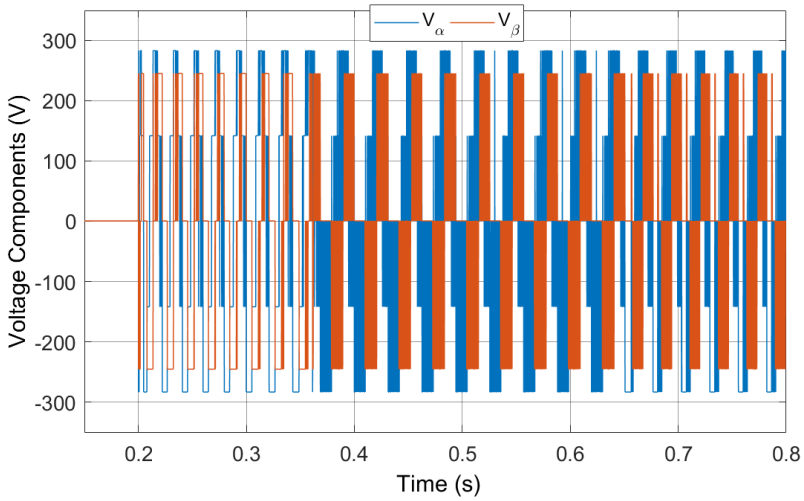

Fig. 5.12. Stator voltage components of FLDTC

5.2.2 Transient Behavior under a Load Change

In this section, four control schemes were compared when drive is functioning at a different operating condition. The drive is subjected to a sudden load change at 0.9s from 2 Nm to 6 Nm at 100 rad/s speed. Performances of the selected schemes are illustrated in Fig. 5.13 (a) – Fig. 5.13 (c). Compared to the CDTC without SA, SMDTC with SA and FLDTC with SA exhibit faster response during the transient period. As depicted in Fig. 5.13, the transient time of CDTC without SA, SMDTC with SA and FLDTC with SA are 1.098s, 0.905s and 0.903s respectively.

Moreover, FL scheme displays a faster response when compared to the SM scheme with a lower torque ripple at the steady state. The FLDTC with SA shows 0.67 Nm ripple while CDTC without SA shows 1.475 Nm ripple at steady state. In addition, time spent

during initial transient and during step load change are summarized in Table 5.1. Hence, it is concluded from the obtained results that FLDTC with SA scheme provides better torque response during load transients.

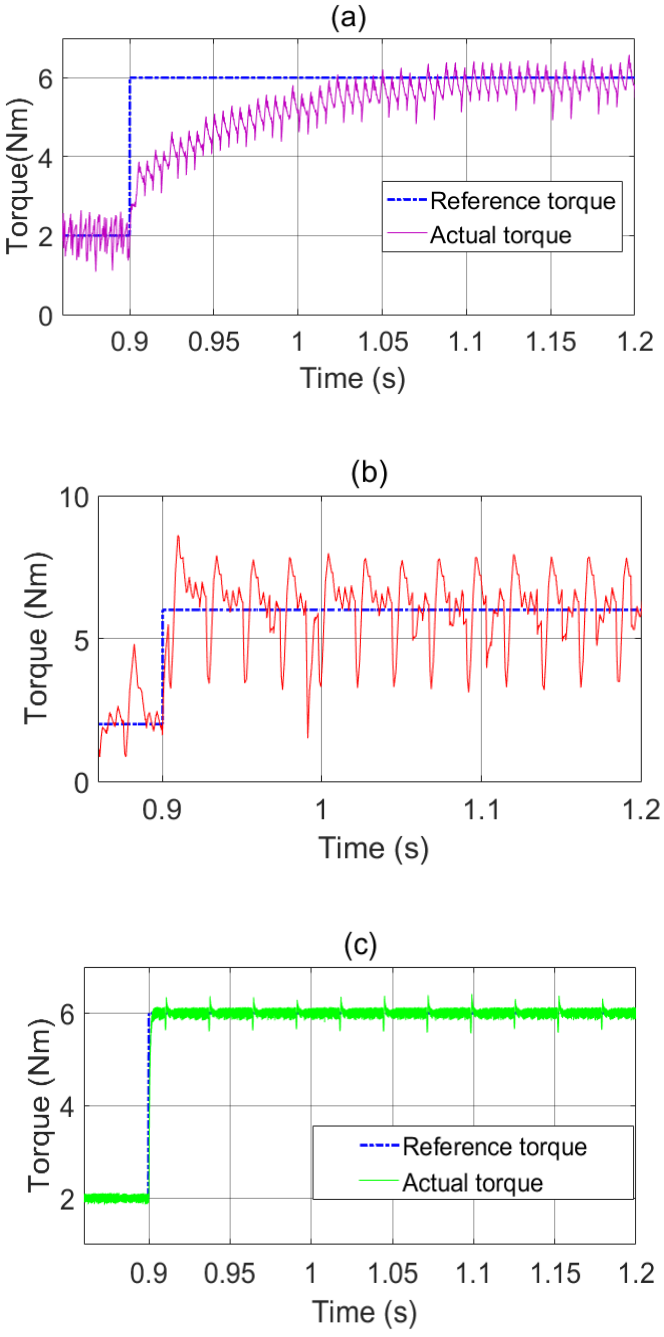

Fig. 5.13. Electromagnetic torque response for load variation (a) CDTC without SA (b) SMDTC with SA (c) FLDTC with SA

5.2.3 Transient Behavior under a Speed Change

The conventional and proposed controllers have been compared during transient stage by means of reference speed change from 100 rad/s to 80 rad/s. The change in the speed is applied at a time t = 1s. Fig. 5.14 (a) – (h) show the variation of the speed and torque response of the induction machine with different control algorithms.

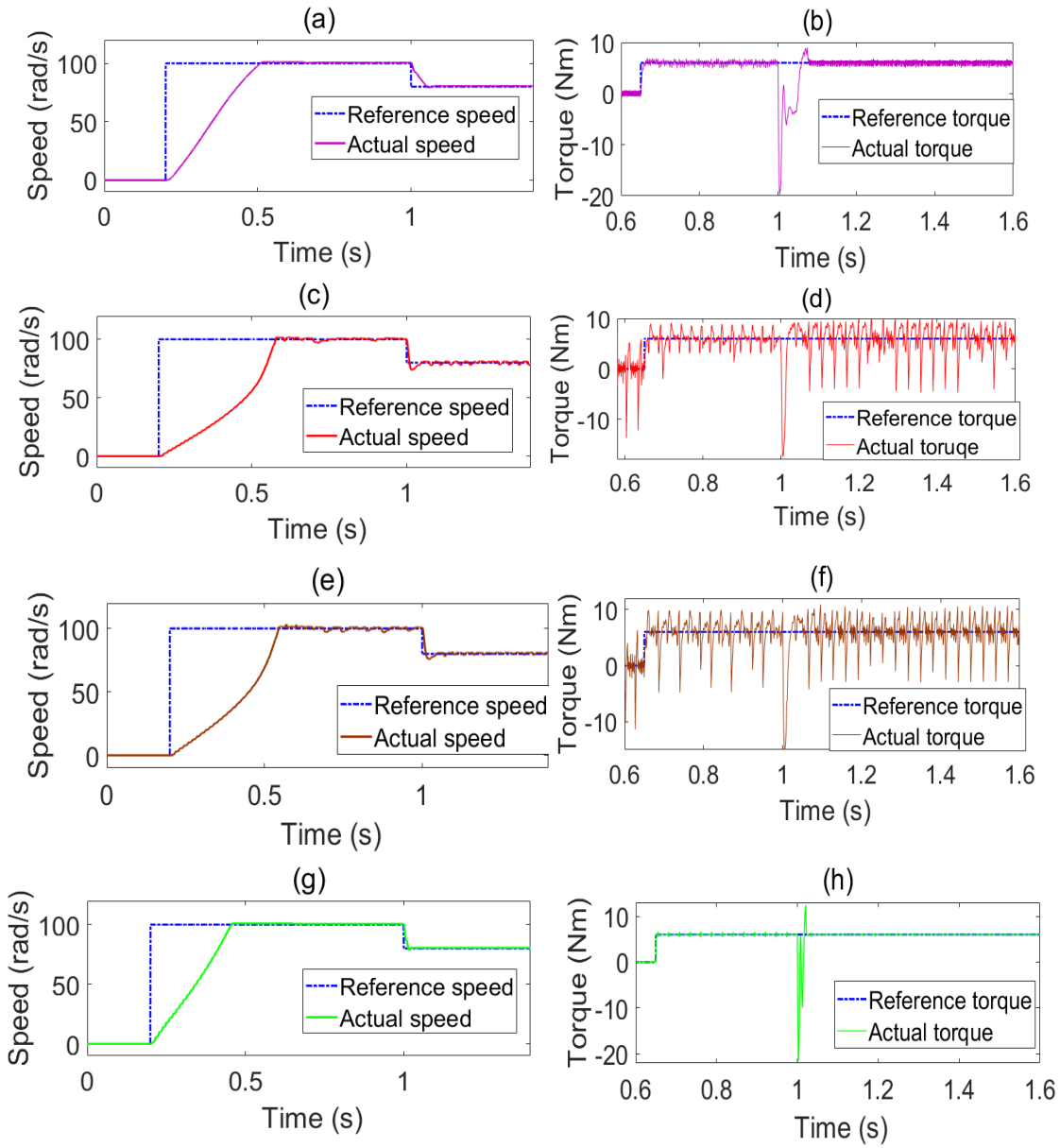

Fig. 5.14 Speed and torque response for step speed change (a) Speed CDTC (b) Torque CDTC (c) Speed CDTC with SA (d) Torque CDTC with SA (e) Speed SMDTC with SA (f) Torque SMDTC with SA (g) Speed FLDTC with SA (h) Torque FLDTC with SA

Due to the sudden drop of the speed reference, the electromagnetic torque generated by the motor undergoes an abrupt undershoot. Fig. 5.14 (a) and (b) show the speed and the torque response of the CDTC drive without SA under speed change. As observed from the Fig. 5.14 (a) and (b), speed reaches the desired stepped down speed at t = 1.08s and the internally generated torque of the motor experiences a significant undershoot followed by slight overshoot before recovering back to its initial state. The DTC drives designed with SA strategy exhibit a significantly lower transient period under the speed change.

The transient time of CDTC with SA, SMDTC with SA, and FLDTC with SA are 1.008s, 1.01s, and 1.009s. Hence, the proposed controllers, as described in Fig. 5.14 (c) – (h), have attained new operating state of the motor within one-tenth of the time lapse of the conventional drive. Further, the proposed controller with FL technique guarantees a lower ripple in torque response while ensuring fast dynamics.

5.2.4 Drive performance under a Voltage Sag Condition

Faults in power system could result in a sudden voltage dip for a short time extent. These under voltage scenarios can disturb the steady operation of the drive system which is interfaced with low voltage bus. The performances of the proposed drives under a voltage sag incident were explored in this test case. 55% of voltage sag is applied to the drives after each of them attained steady state. During the fault, drive experience a lower voltage for 100 ms period starting from t = 1s to t = 1.1s.

Fig. 5.15 shows the speed response of each controller. As illustrated in Fig. 5.15 the speed of the CDTC without SA drops to a value of 50.45 rad/s as voltage drops. Next, it jumps back to the desired speed in 0.201s once the fault is cleared. The controllers that are designed with SA strategy exhibit a lower speed drop and a smaller recovery time when compared to the driver implemented without SA. Maximum speed drop and the recovery time of FLDTC are 30.16 rad/s and 1.184 s, and corresponding values of SMDTC are 37.9 rad/s and 1.327s. A summary of the obtained results is displayed in Table 5.1.

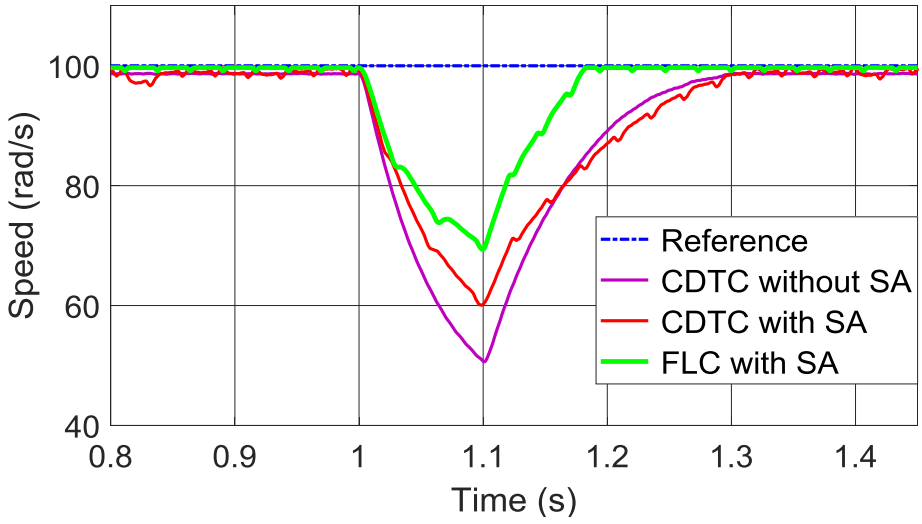

Fig. 5.15. Speed response under a voltage sag condition for different controllers

TABLE 5.1

Summary of the Test Cases

	CDTC Without SA	*CDTC With SA*	*SMDTC With SA*	*FLDTC With SA*
Initial Torque transient response time (s)	0.015	0.008	0.003	0.001
Torque Transient response time during load change(s)	0.198	0.006	0.005	0.003
Speed recovery time under voltage sag (s)	0.201	0.242	0.227	0.084
Maximum speed drop under voltage sag (rad/s)	49.55	37.92	37.45	30.16
Average steady state torque ripple during load change (Nm)	1.63	5.87	4.68	0.39

5.2.5 Sensitivity Analysis of the Weighting Factors in FL Controller

As explained in Fig. 4.3, FL based DTC utilizes two PI type fuzzy controllers in the stator flux control loop and the electromagnetic torque control loop. Each controller has two weighting factors. The weighting factor in the integral path denotes as W_{k_i} and the one in the proportional path denotes as W_{k_p}. These weighting factors have an impact on the dynamic stability, convergence rate, steady-state response, and the overshoot in output response of stator flux and torque controllers. In this study, it was intended to evaluate the sensitivity of two weighting factors associated with the torque control loop. Similar behavior can be expected in flux control loop as well.

The optimal values of the weighting factors W_{k_i} and W_{k_p} are 0.8 and 20, which have been employed in entire the simulation. For the previous test cases, these values were selected by trial and error method in order to get a better compromise between aforementioned design criteria. The torque response trajectory variation for higher and lower values of weighting factors with regard to the optimal values have been investigated. The test case values for W_{k_i} and W_{k_p} are selected arbitrarily in order to demonstrate clear deviation in regards to those obtained with optimal values. Fig. 5.16 and Fig. 5.17 show the torque response trajectories with optimal weights and arbitrary weights in FL control loop.

The torque response for different W_{k_i} while keeping the W_{k_p}at its optimal value is plotted in Fig. 5.16. As illustrated in the Fig. 5.16, a large enough value for W_{k_i} increases the convergence rate of the torque permitting fast tracking of the desired load torque. However, larger values of W_{k_i} might trigger a slight overshoot in torque response. In this case, 6% of overshoot can be observed with a higher W_{k_i} value.

The variation of the torque response with respect to different W_{k_p} and optimal W_{k_i} is depicted in Fig. 5.17. Setting a lower value for W_{k_p} introduces a considerable ripple in the steady state torque response, which is an undesirable characteristic for the torque controller. The steady state torque ripple with W_{k_p}= 0.01 is 13.7%, which is higher than that of the optimal gain value.

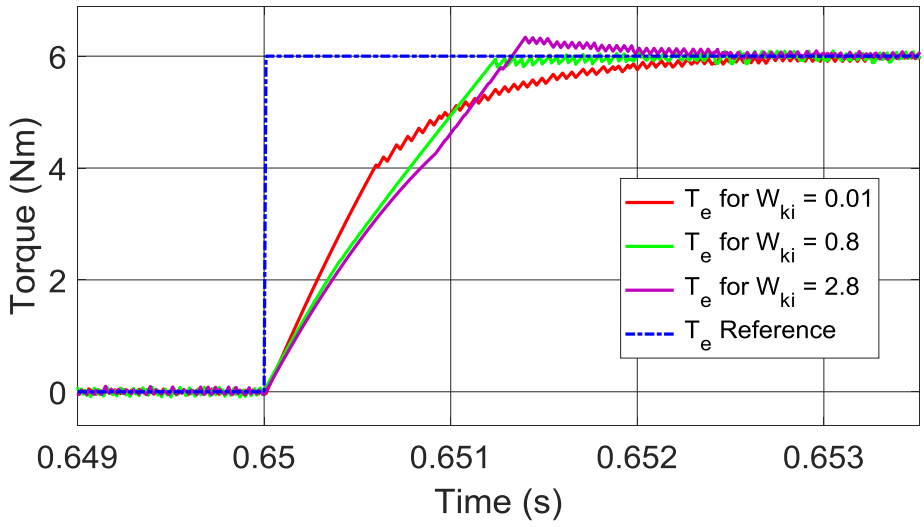

Fig. 5.16. Variation of the torque response for different W_{k_i} values

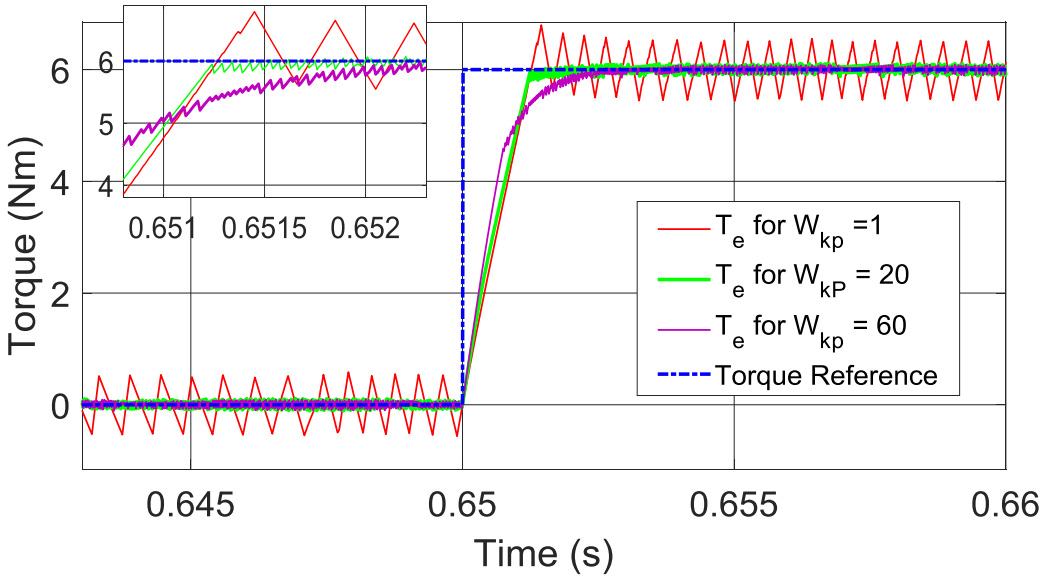

Fig. 5.17. Variation of the torque response for different W_{k_p} values

CHAPTER VI

CONCLUSION

6.1 Concluding Remarks

DTC has its roots in field oriented control and direct self control. In its basic form, DTC utilizes a three level hysteresis torque controller, a two level hysteresis flux controller, and the stator flux position to select the inverter voltage vector from a predefined switching table. In this thesis, an improved sector advancing (SA) algorithm has been developed together with two nonlinear adaptation mechanisms to improve the dynamic performance of the DTC drive. Two mechanisms namely, sliding mode (SM) and fuzzy logic (FL) have been used to reconstruct the conventional torque and flux control loop ensuring stability with fast dynamics. An extensive review of literature has been performed to investigate the previous work in the related field. Complete mathematical modeling of the three-phase induction motor in two axes stationary reference frame has been given.

Control architecture of the proposed DTC methodology combining SA technique, FL, and SM has been presented. The effectiveness of the proposed method was evaluated in MATLAB/Simulink. Several test cases were carried out to examine the performances of the proposed DTC drive with and without SA strategy and to further improve the characteristics of the drive by incorporating the SM and FL techniques. According to the obtained results, initial torque transient response time of the proposed controller with FL and SA strategies has improved 93% when compared to the CDTC without SA, and 87% with respect to the CDTC with SA. During load application, each controller has taken different transient times based on the controller dynamics. However, FLDTC with SA has demonstrated the best performance with 50% shorter time with respect to the CDTC with

SA. Moreover, under the voltage sag condition, the controllers designed with different control techniques have demonstrated different speed recovery times and the maximum speed drops. The maximum speed drop has observed from the CDTC without SA and it is 39 % higher than that of FLDTC. The maximum speed drop of CDTC with SA is 20% higher than the FLDTC.

In voltage sag test case, after the fault is cleared, each controller tries to follow the desired speed. The speed recovery time of the FLDTC with SA is 65 % lower than that of the CDTC with SA. The simulation results demonstrate that the proposed strategy has a significant impact on performance when compared to the CDTC drive. The SA topology displays better performance during the transient, as well as under sudden voltage drop. Some inherent drawback of SA technique, such as the steady state chattering problem, has been reduced with the aid of FL strategy.

The proposed control strategies for the DTC drives can be utilized in practical applications where instantaneous torque increment is required. Traction drives and electrical vehicles are some of the application that require better torque regulation within smaller time period.

6.2 Novelty of the proposed approach

The proposed approach has been used a combined strategies of sector advancing, sliding mode and fuzzy logic control to improve the transient and the steady state performance of the conventional DTC drive. Two novel controllers have been designed by using; 1) sliding mode and sector advancing 2) fuzzy logic and sector advancing. Sliding mode and fuzzy logic controllers improve the torque and flux control loops while sector advancing concept is utilized to enhance the process of voltage vector selection. Moreover, another newly added feature of the design is that the PI type fuzzy controller gains have been changed adaptively according to the magnitudes of torque and flux errors.

6.3 Future Scope

This study focused to improve the dynamic performance of the CDTC drive while reducing the undesired torque ripple. This was achieved by incorporating two advanced

nonlinear control techniques; sliding mode and fuzzy logic combined with the SA concept. However, the steady state performance can further be improved by introducing a hybrid fuzzy controller with two different fuzzy controllers one at the transient state and the other one during the steady state. A simple switching mechanism can be developed to switch between two controllers. This method will reduce undesired the steady state pulsation introduced by the SA strategy while preserving its merits during the transient period.

The study can be further extended to deploy in sensorless drives by introducing a rotor speed observer. This lessens problems such as drive complexity, low reliability due to the sensors and cable, increased axial length of the machine and electromagnetic noise interference. The observer can be designed with the aid of modern control theory such as Kalman filtering or intelligent control methods. In DTC scheme, at each sampling instant required voltage vector is computed based on the error between estimated and the desired stator flux. The estimated stator flux is directly estimated using the stator resistance. Any variation of stator resistance results an error in the flux estimation process. Hence, a stator resistance adaptation mechanism can be introduced to the DTC drive to avoid such issue.

REFERENCES

[1] A. M. Bazzi, A. Dominguez-Garcia, and P. T. Krein, "Markov Reliability Modeling for Induction Motor Drives Under Field-Oriented Control," *IEEE Trans. Power Electron.,* vol. 27, no. 2, pp. 534-546, 2012.

[2] S. Sathiakumar, S. Biswas, and J. Vithayathil, "Microprocessor-based field-oriented control of a CSI-fed induction motor drive," *IEEE Trans. Ind. Electron.,* no. 1, pp. 39-43, 1986.

[3] R. H. Kumar, A. Iqbal, and N. C. Lenin, "Review of recent advancements of direct torque control in induction motor drives–a decade of progress," *IET Power Electronics,* 2017.

[4] Y.-S. Lai and J.-C. Lin, "New hybrid fuzzy controller for direct torque control induction motor drives," *IEEE Trans. Power Electron.,* vol. 18, no. 5, pp. 1211-1219, 2003.

[5] K.-B. Lee, S.-H. Huh, J.-Y. Yoo, and F. Blaabjerg, "Performance improvement of DTC for induction motor-fed by three-level inverter with an uncertainty observer using RBFN," *IEEE Trans. Energy Convers.,* vol. 20, no. 2, pp. 276-283, 2005.

[6] J. N. Nash, "Direct torque control, induction motor vector control without an encoder," *IEEE Trans. Ind. Appl.,* vol. 33, no. 2, pp. 333-341, 1997.

[7] B. K. Bose, *Power electronics and motor drives: advances and trends*. Elsevier, 2010.

[8] R. A. Keswani, H. M. Suryawanshi, and M. S. Ballal, "Multi-resolution analysis for converter switch faults identification," *IET Power Electronics,* vol. 8, no. 5, pp. 783-792, 2015.

[9] R. Teodorescu, F. Blaabjerg, J. K. Pedersen, E. Cengelci, and P. N. Enjeti, "Multilevel inverter by cascading industrial VSI," *IEEE Transactions on Industrial Electronics,* vol. 49, no. 4, pp. 832-838, 2002.

[10] B. K. Bose, "Scalar decoupled control of induction motor," *IEEE Trans. Ind. Appl.,* no. 1, pp. 216-225, 1984.

[11] T. F. Chan and K. Shi, *Applied intelligent control of induction motor drives*. John Wiley & Sons, 2011.

[12] C. Lascu, I. Boldea, and F. Blaabjerg, "Direct torque control of sensorless induction motor drives: a sliding-mode approach," *IEEE Trans. Ind. Appl.,* vol. 40, no. 2, pp. 582-590, 2004.

[13] S. J. Evangeline and S. Suresh Kumar, "Minimization of Torque Ripple in Switched Reluctance Motor Drive–A Review," *Advanced Electrical and Electronics Engineering,* pp. 287-294, 2011.

[14] V. Utkin, J. Guldner, and J. Shi, *Sliding mode control in electro-mechanical systems*. CRC press, 2009.

[15] G. Kenne, T. Ahmed-Ali, F. Lamnabhi-Lagarrigue, and A. Arzande, "Real-time speed and flux adaptive control of induction motors using unknown time-varying rotor resistance and load torque," *IEEE Trans. Energy Convers. ,* vol. 24, no. 2, pp. 375-387, 2009.
[16] C. Lascu, S. Jafarzadeh, M. S. Fadali, and F. Blaabjerg, "Direct torque control with feedback linearization for induction motor drives," *IEEE Trans. Power Electron.,* vol. 32, no. 3, pp. 2072-2080, 2017.
[17] Z. Zhang, R. Tang, B. Bai, and D. Xie, "Novel direct torque control based on space vector modulation with adaptive stator flux observer for induction motors," *IEEE Trans. Magn.,* vol. 46, no. 8, pp. 3133-3136, 2010.
[18] M. Hajian, J. Soltani, G. A. Markadeh, and S. Hosseinnia, "Adaptive nonlinear direct torque control of sensorless IM drives with efficiency optimization," *IEEE Trans. Ind. Electron.,* vol. 57, no. 3, pp. 975-985, 2010.
[19] S. M. J. R. Fatemi, N. R. Abjadi, J. Soltani, and S. Abazari, "Speed sensorless control of a six-phase induction motor drive using backstepping control," *IET Power Electron.,* vol. 7, no. 1, pp. 114-123, 2014.
[20] I. Takahashi and T. Noguchi, "A new quick-response and high-efficiency control strategy of an induction motor," *IEEE Trans. Ind. Appl.,* no. 5, pp. 820-827, 1986.
[21] D. Casadei, G. Serra, A. Tani, L. Zarri, and F. Profumo, "Performance analysis of a speed-sensorless induction motor drive based on a constant-switching-frequency DTC scheme," *IEEE Trans. Ind. Appl.,* vol. 39, no. 2, pp. 476-484, 2003.
[22] M. Comanescu, "Design and implementation of a highly robust sensorless sliding mode observer for the flux magnitude of the induction motor," *IEEE Trans. Energy Convers.,* vol. 31, no. 2, pp. 649-657, 2016.
[23] P. Correa, M. Pacas, and J. Rodriguez, "Predictive torque control for inverter-fed induction machines," *IEEE Trans. Ind. Electron.,* vol. 54, no. 2, pp. 1073-1079, 2007.
[24] M. Habibullah, D. D.-C. Lu, D. Xiao, and M. F. Rahman, "A simplified finite-state predictive direct torque control for induction motor drive," *IEEE Trans. Ind. Electron.,* vol. 63, no. 6, pp. 3964-3975, 2016.
[25] N. R. N. Idris and A. H. M. Yatim, "An improved stator flux estimation in steady-state operation for direct torque control of induction machines," *IEEE Trans. Ind. Appl.,* vol. 38, no. 1, pp. 110-116, 2002.
[26] C. Lascu, I. Boldea, and F. Blaabjerg, "Variable-structure direct torque control-a class of fast and robust controllers for induction machine drives," *IEEE Trans. Ind. Electron.,* vol. 51, no. 4, pp. 785-792, 2004.
[27] H.-J. Shieh and K.-K. Shyu, "Nonlinear sliding-mode torque control with adaptive backstepping approach for induction motor drive," *IEEE Trans. Ind. Electron.,* vol. 46, no. 2, pp. 380-389, 1999.
[28] M. Uddin and M. Hafeez, "FLC-based DTC scheme to improve the dynamic performance of an IM drive," *IEEE Trans. Ind. Appl.,* vol. 48, no. 2, pp. 823-831, 2012.
[29] S.-C. Tan, Y.-M. Lai, and C.-K. Tse, *Sliding mode control of switching power converters: techniques and implementation*. CRC press, 2011.

[30] A. A. Naassani, E. Monmasson, and J.-P. Louis, "Synthesis of direct torque and rotor flux control algorithms by means of sliding-mode theory," *IEEE Trans. Ind. Electron.,* vol. 52, no. 3, pp. 785-799, 2005.
[31] M. H. Hebert, C. E. Thorpe, and A. Stentz, *Intelligent unmanned ground vehicles: autonomous navigation research at Carnegie Mellon*. Springer Science & Business Media, 2012.
[32] T. Duriez, S. L. Brunton, and B. R. Noack, *Machine Learning Control-Taming Nonlinear Dynamics and Turbulence*. Springer, 2017.
[33] N. Siddique, *Intelligent control: a hybrid approach based on fuzzy logic, neural networks and genetic algorithms*. Springer, 2013.
[34] L. Romeral, A. Arias, E. Aldabas, and M. G. Jayne, "Novel direct torque control (DTC) scheme with fuzzy adaptive torque-ripple reduction," *IEEE Trans. Ind. Electron.,* vol. 50, no. 3, pp. 487-492, 2003.
[35] A. Saghafinia, H. W. Ping, M. N. Uddin, and K. S. Gaeid, "Adaptive fuzzy sliding-mode control into chattering-free IM drive," *IEEE Trans. Ind. Appl.,* vol. 51, no. 1, pp. 692-701, 2015.
[36] C. Lascu, I. Boldea, and F. Blaabjerg, "A modified direct torque control for induction motor sensorless drive," *IEEE Trans. Ind. Appl.,* vol. 36, no. 1, pp. 122-130, 2000.
[37] S. Ryvkin, R. Schmidt-Obermoeller, and A. Steimel, "Sliding-mode-based control for a three-level inverter drive," *IEEE Trans. Ind. Electron.,* vol. 55, no. 11, pp. 3828-3835, 2008.
[38] Z. Yan, C. Jin, and V. Utkin, "Sensorless sliding-mode control of induction motors," *IEEE Trans. Ind. Electron.,* vol. 47, no. 6, pp. 1286-1297, 2000.
[39] H.-u. Rehman, A. Derdiyok, M. K. Guven, and L. Xu, "A new current model flux observer for wide speed range sensorless control of an induction machine," *IEEE Trans. Ind. Electron.,* vol. 17, no. 6, pp. 1041-1048, 2002.
[40] M. Ouhrouche, R. Errouissi, A. M. Trzynadlowski, K. A. Tehrani, and A. Benzaioua, "A novel predictive direct torque controller for induction motor drives," *IEEE Trans. Ind. Electron.,* vol. 63, no. 8, pp. 5221-5230, 2016.
[41] M. Nemec, D. Nedeljkovic, and V. Ambrozic, "Predictive torque control of induction machines using immediate flux control," *IEEE Trans. Ind. Electron.,* vol. 54, no. 4, pp. 2009-2017, 2007.
[42] H. Miranda, P. Cortés, J. I. Yuz, and J. Rodríguez, "Predictive torque control of induction machines based on state-space models," *IEEE Trans. Ind. Electron.,* vol. 56, no. 6, pp. 1916-1924, 2009.
[43] P. V. R. L. Narasimham, A. V. R. S. Sarma, and E. Vargilkumar, "An Improvement in Dynamic Response of a Direct Torque Controlled Induction Motor Using Sector Advancing Technique," in *Proc. 16th NATIONAL POWER SYSTEMS CONFERENCE*, India, 2010.
[44] A. M. Trzynadlowski, *Control of induction motors*. Elsevier, 2000.
[45] P. Krause, O. Wasynczuk, S. D. Sudhoff, and S. Pekarek, *Analysis of electric machinery and drive systems*. John Wiley & Sons, 2013.
[46] B. Robyns, B. Francois, P. Degobert, and J. P. Hautier, "Vector control of induction machines," in *Vector Control of Induction Machines*: Springer, 2012, pp. 75-121.

[47] R. Marino and P. Tomei, *Nonlinear control design: geometric, adaptive, and robust*. Prentice Hall London, 1995.
[48] N. R. N. Idris and A. H. M. Yatim, "Direct torque control of induction machines with constant switching frequency and reduced torque ripple," *IEEE Trans. Ind. Electron.,* vol. 51, no. 4, pp. 758-767, 2004.
[49] Y.-S. Lai and J.-H. Chen, "A new approach to direct torque control of induction motor drives for constant inverter switching frequency and torque ripple reduction," *IEEE Trans. Energy Convers. ,* vol. 16, no. 3, pp. 220-227, 2001.
[50] Y. Bai, H. Zhuang, and D. Wang, *Advanced fuzzy logic technologies in industrial applications*. Springer Science & Business Media, 2007.
[51] L. A. Amézquita-Brooks, J. Licéaga-Castro, E. Licéaga-Castro, and C. E. Ugalde-Loo, "Induction Motor Control: Multivariable Analysis and Effective Decentralized Control of Stator Currents for High-Performance Applications," *IEEE Trans. Ind. Electron.,* vol. 62, no. 11, pp. 6818-6832, 2015.
[52] Y.-S. Lai and J.-H. Chen, "A new approach to direct torque control of induction motor drives for constant inverter switching frequency and torque ripple reduction," *IEEE Transactions on Energy Conversion,* vol. 16, no. 3, pp. 220-227, 2001.
[53] J. K. Pandit, M. V. Aware, R. V. Nemade, and E. Levi, "Direct Torque Control Scheme for a Six-Phase Induction Motor With Reduced Torque Ripple," *IEEE Trans. Power Electron.,* vol. 32, no. 9, pp. 7118-7129, 2017.
[54] K. B. Bimal, *Modern power electronics and AC drives*. 2002.

APPENDIX

List of motor specifications and parameter values.

Parameter	Value
Voltage	220 V
Rated power	3 hp
Rated speed	1710 rpm
Number of poles	4
Stator resistance	0.435 Ω
Rotor resistance	0.816 Ω
Stator inductance	0.0713 H
Rotor inductance	0.0713H
Mutual inductance	0.0693H
Inertia	0.0088 Nm^2

VITA

AMALI DEHIGOLLE GEDARA

Candidate for the Degree of

Master of Science

Thesis: MODIFIED DIRECT TORQUE CONTROL OF INDUCTION MOTOR DRIVES

Major Field: Electrical Engineering

Biographical:

Education:

Completed the requirements for the Master of Science in Electrical Engineering at Oklahoma State University, Stillwater, Oklahoma in July 2018.

Completed the requirements for the Bachelor of Science in Electrical & Electronics Engineering at University of Peradeniya, Kandy, Sri Lanka in 2014.

Experience:

Graduate Research Assistant, Physics Department, Oklahoma State University, January 2018 - July 2018.
Graduate Research Assistant, Department of Electrical and Computer Engineering, Oklahoma State University, January 2017 - December 2017.
Electrical Engineer, Central Engineering Consultancy Bureau, Sri Lanka, September 2015 – June 2016.
Teaching Assistant, University of Peradeniya, Sri Lanka, October 2014 – September 2015.

Professional Memberships:

Graduate Student Member: IEEE
Graduate Student Member: IEEE Women in Engineering
Associate Member: IESL